2002-12

A numerical study of combined convective and radiative heat transfer in a rocket engine combustion chamber

Savur, Mehmet Koray

Monterey, California. Naval Postgraduate School

NAVAL POSTGRADUATE SCHOOL
Monterey, California

THESIS

A NUMERICAL STUDY OF COMBINED CONVECTIVE AND RADIATIVE HEAT TRANSFER IN A ROCKET ENGINE COMBUSTION CHAMBER

by

Mehmet Koray Savur

December 2002

Thesis Advisor: Ashok Gopinath

Approved for public release; distribution is unlimited.

THIS PAGE INTENTIONALLY LEFT BLANK

REPORT DOCUMENTATION PAGE

Form Approved OMB No. 0704-0188

1. AGENCY USE ONLY *(Leave blank)*	2. REPORT DATE	3. REPORT TYPE AND DATES COVERED
	December 2002	Master's Thesis

4. TITLE AND SUBTITLE A Numerical Study of Combined Convective and Radiative Heat Transfer in a Rocket Engine Combustion Chamber

5. FUNDING NUMBERS

6. AUTHOR (S) Savur, Mehmet Koray

7. PERFORMING ORGANIZATION NAME(S) AND ADDRESS(ES)
Naval Postgraduate School
Monterey, CA 93943-5000

8. PERFORMING ORGANIZATION REPORT NUMBER

9. SPONSORING / MONITORING AGENCY NAME(S) AND ADDRESS(ES)

10. SPONSORING/MONITORING AGENCY REPORT NUMBER

11. SUPPLEMENTARY NOTES The views expressed in this thesis are those of the author and do not reflect the official policy or position of the U.S. Department of Defense or the U.S. Government.

12a. DISTRIBUTION / AVAILABILITY STATEMENT
Approved for public release; distribution is unlimited.

12b. DISTRIBUTION CODE

13. ABSTRACT *(maximum 200 words)*

A numerical study was conducted to predict the combined convective and radiative heat transfer rates on the walls of a small aspect ratio cylinder representative of the scaled model of a rocket engine combustion chamber. A high-temperature, high-pressure environment was simulated in the cylinder, with gas velocities at low subsonic levels typical of the conditions leading to the entrance of the nozzle section of a rocket engine. The composition of the gases in the cylinder was determined from the TEP program for the burning of rocket fuel at typical values of the O/F ratio. The thrust of the study was to determine the radiative contribution to the heat transfer rate from the hot participating chamber gases to the cooler wall. The calculations were carried out using the commercial CFD package CFDACE, and were first benchmarked against known results in the literature for the simpler case of gray chamber walls and a gray participating medium. The non-gray computations were subsequently carried out using gas absorption coefficient values obtained from the exponential wide band model with the help of the fire-modeling program, RADCAL. The effect of different chamber wall temperatures and gas compositions were examined. The main findings of the study are that the radiative contributions at the high gas temperatures being considered are comparable to the convective values, and strongly spectral in nature. In addition these radiative fluxes were found to be least sensitive to the wall temperature and chamber pressure in the range considered. Furthermore, this radiative contribution reaches a maximum at a unique optimal optical thickness of the gas that lies within the extremes of the optically thin and thick limiting cases.

14. SUBJECT TERMS	15. NUMBER OF PAGES
Radiative Heat Transfer, Rocket Engine, Combustion Chamber, RADCAL, TEP, CFD-ACE, non-gray gas, spectral transmissivity, absorption coefficient	99
	16. PRICE CODE

17. SECURITY CLASSIFICATION OF REPORT	18. SECURITY CLASSIFICATION OF THIS PAGE	19. SECURITY CLASSIFICATION OF ABSTRACT	20. LIMITATION OF ABSTRACT
Unclassified	Unclassified	Unclassified	UL

NSN 7540-01-280-5500 **Standard Form 298 (Rev. 2-89)**
Prescribed by ANSI Std. 239-18

THIS PAGE INTENTIONALLY LEFT BLANK

Approved for public release; distribution is unlimited.

A NUMERICAL STUDY OF COMBINED CONVECTIVE AND RADIATIVE HEAT TRANSFER IN A ROCKET ENGINE COMBUSTION CHAMBER

Mehmet Koray Savur
Lieutenant Junior Grade, Turkish Navy
B.S., Turkish Naval Academy, 1997

Submitted in partial fulfillment of the
requirements for the degree of

MASTER OF SCIENCE IN MECHANICAL ENGINEERING

from the

NAVAL POSTGRADUATE SCHOOL
December 2002

Author: Mehmet Koray Savur

Approved by: Ashok Gopinath
Thesis Advisor

Young W. Kwon
Chairman
Department of Mechanical Engineering

THIS PAGE INTENTIONALLY LEFT BLANK

ABSTRACT

A numerical study was conducted to predict the combined convective and radiative heat transfer rates on the walls of a small aspect ratio cylinder representative of the scaled model of a rocket engine combustion chamber. A high-temperature, high-pressure environment was simulated in the cylinder, with gas velocities at low subsonic levels typical of the conditions leading to the entrance of the nozzle section of a rocket engine. The composition of the gases in the cylinder was determined from the TEP program for the burning of rocket fuel at typical values of the O/F ratio. The thrust of the study was to determine the radiative contribution to the heat transfer rate from the hot participating chamber gases to the cooler wall. The calculations were carried out using the commercial CFD package CFDACE, and were first benchmarked against known results in the literature for the simpler case of gray chamber walls and a gray participating medium. The non-gray computations were subsequently carried out using gas absorption coefficient values obtained from the exponential wide band model with the help of the fire-modeling program, RADCAL. The effect of different chamber wall temperatures and gas compositions were examined. The main findings of the study are that the radiative contributions at the high gas temperatures being considered are comparable to the convective values, and strongly spectral in nature. In addition these radiative fluxes were found to be least sensitive to the wall temperature and chamber pressure in the range considered. Furthermore, this radiative

contribution reaches a maximum at a unique optimal optical thickness of the gas that lies within the extremes of the optically thin and thick limiting cases.

TABLE OF CONTENTS

THIS PAGE INTENTIONALLY LEFT BLANK

LIST OF FIGURES

LIST OF TABLES

THIS PAGE INTENTIONALLY LEFT BLANK

ACKNOWLEDGEMENTS

I would like to thank Professor Ashok Gopinath for his continuous support, motivation and guidance throughout this work as well as making this research challenging. I am deeply indebted to you for the months you have devoted to this thesis research and the patience that you showed throughout the course of my work.

Special thanks to Dr. Christopher M. Brophy and his colleagues for their valuable input.

Finally, I also take this opportunity to acknowledge my dear wife, my better half Gulsev, for her understanding, sacrifice, love and support, and our lovely baby Mete for keeping me awake while completing this work as well as making my life better and better day by day.

THIS PAGE INTENTIONALLY LEFT BLANK

I. INTRODUCTION

The heat transfer behavior in many high temperature applications involves a combination of radiative and convective heat transfer modes. Analyses of such applications are often complicated by irregular geometry, turbulence, and combustion.

Radiation within a medium containing products of combustion is dependent upon the temperature and concentrations through the entire field. The energy is distributed across the infrared spectrum in a highly nonlinear fashion. This greatly complicates modeling of the heat transfer within such high temperature environments.

Gaseous radiation is particularly relevant to heat transfer in combustion chambers burning carbon, hydrogen, or hydrocarbon fuels. Absorption and emission by carbon dioxide, water vapor and other products of combustion is of particular concern due to their strong radiative participation.

This thesis deals with the characteristics of combined convective and radiative heat transfer rates on the walls of a small aspect ratio cylinder representative of the scaled model of a rocket engine combustion chamber.

THIS PAGE INTENTIONALLY LEFT BLANK

II. BACKGROUND & MOTIVATION

The flow and heat transfer behavior in a rocket engine is crucial in determining its performance as well as its thermal signature.

The schematic of a typical rocket engine is shown in Figure 1.

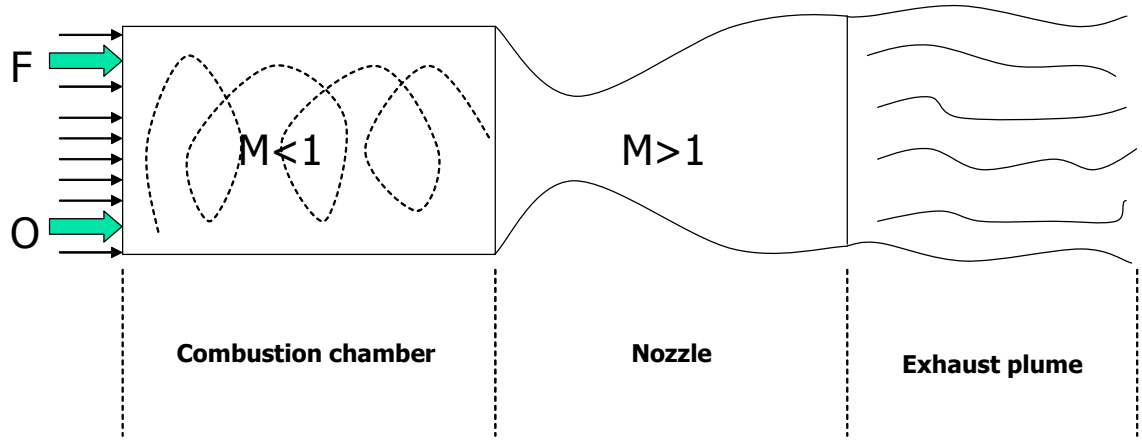

Figure 1. Rocket Engine Schematic

There are three main sections in a rocket engine. The first is the combustion chamber, in which oxygen as oxidizer and fuel, i.e. RP1, are ignited and a high-temperature, high pressure environment is created. Gas velocities are at low subsonic levels typical of the conditions leading to the nozzle section. In the nozzle the flow is accelerated to supersonic velocities and is ejected in the exhaust plume.

For this phase of the research program, this thesis focuses only on the heat transfer behavior in the combustion chamber and this thesis provides modeling and

numerical support to ongoing Air Force Research Laboratory sponsored research program.

III. PROBLEM DESCRIPTION

A. THE MODEL PROBLEM

Detailed schematic of scaled-down model of cylindrical combustion chamber as used in the experimental program is shown in Figure 2.

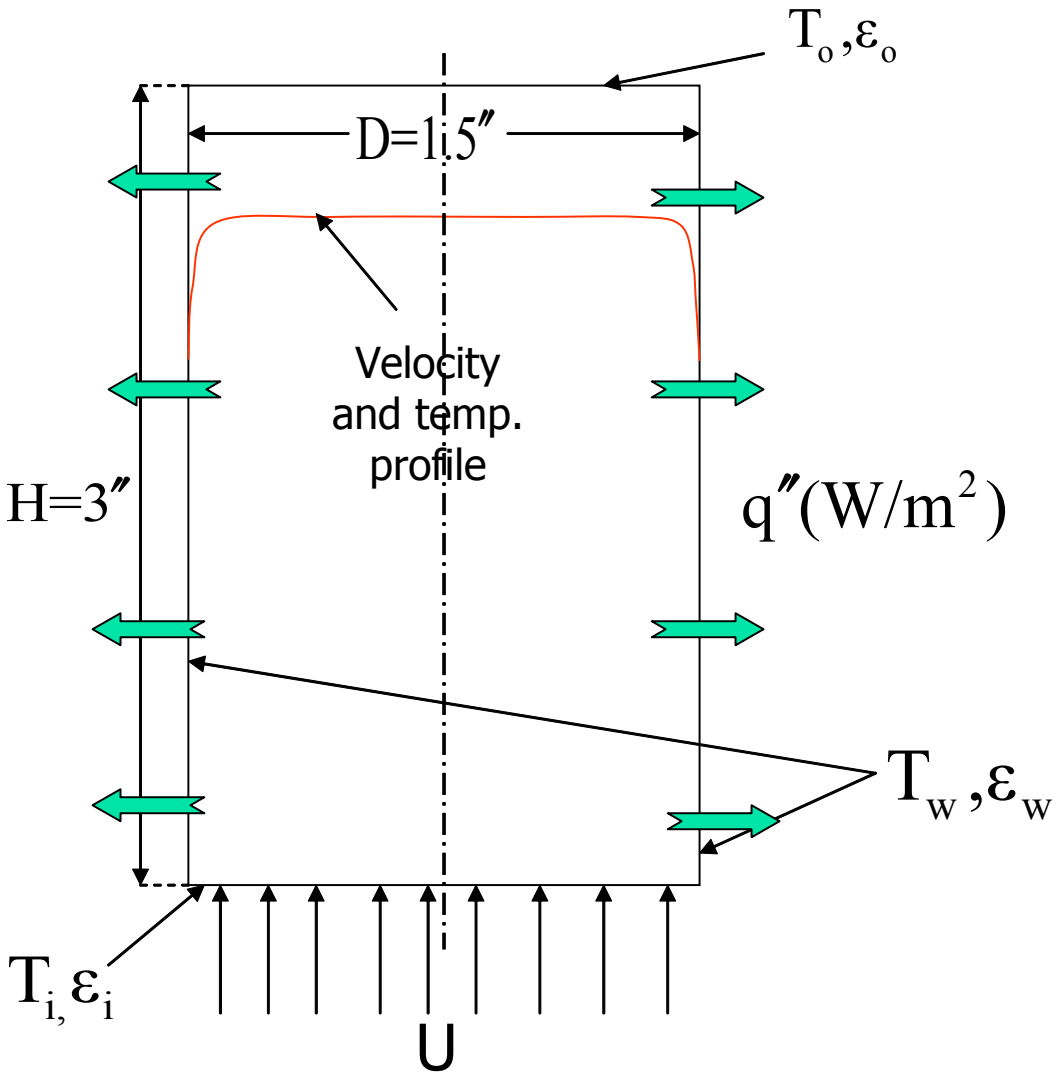

Figure 2. Detailed Schematic of Scaled-down Model

The scaled model of the combustion chamber consists of a participating (absorbing and emitting but non-scattering) gray/non-gray gas flowing through a circular duct in the entrance developing region of flow. The gas is assumed to enter the duct at a uniform velocity and high temperature and pressure. The duct wall is treated as isothermal with temperatures ranging from 400 °K to 800 °K. A schematic diagram of the model is shown in Figure 2.1. The inner diameter of the duct is 1.5″, and its length is 3″. RP1 is the fuel being burned, while oxygen is used as oxidizer. The products of the combustion process are determined based on an O/F value of 3 which is typical of the chamber. The actual combustion is not modeled in this initial study, although its net effect is represented as a well mixed core of the constituents with core temperatures ranging from 1500°K to 3500°K for use in this parametric study. The inlet fluid velocity to the duct is taken to be uniform at a value corresponding to a low subsonic Mach number.

B. GAS RADIATION

As per the laws of quantum mechanics, molecular gases can emit or absorb photons to varying degrees at an infinite set of distinct wavenumbers or frequencies. No spectral line can be truly monochromatic; rather, absorption or emission occurs over a tiny but finite range of wavenumbers. The results are broadened spectral lines that have their centers (maxima) at the wavenumber predicted by quantum mechanics. Three most important phenomena that cause broadening of spectral lines are

collision broadening, natural line broadening, and Doppler broadening.

A single spectral line at a spectral position is characterized by its intensity and its line half-width. However, a vibration-rotation band has many closely spaced spectral lines that may overlap considerably. The absorption coefficient for the entire band is found by adding the absorption coefficients for single lines.

$$\kappa_\eta = \sum_j \kappa_{\eta j} \tag{2.1}$$

All spectral integrations may be reduced to two cases,

$$\int_0^\infty \kappa_\eta I_{(b)\eta} d\eta \quad \text{and} \quad \int_0^\infty I_{(b)\eta}[1-\exp(-\int_0^s \kappa_\eta ds)]d\eta \tag{2.2}$$

where $I_{(b)\eta}$ denotes that either $I_{b\eta}$ or I_η can occur.

Since the local radiation intensity is due to emission from all locations within the medium and the bounding walls, it can be expected to be smooth. It is further smoothed by absorption and scattering. As a result, the previous equation simplifies to

$$\int_0^\infty I_{(b)\eta}\left\{\frac{1}{\Delta\eta}\int_{\eta-\Delta\eta/2}^{\eta+\Delta\eta/2}\kappa_\eta d\eta'\right\}d\eta \tag{2.3}$$

and

$$\int_0^\infty I_{(b)\eta}\left\{\frac{1}{\Delta\eta}\int_{\eta-\Delta\eta/2}^{\eta+\Delta\eta/2}[1-\exp(-\int_0^s \kappa_\eta ds)]d\eta'\right\}d\eta \tag{2.4}$$

In order to find narrow band values of the absorption coefficient and the emissivity, required information about the spacing of the individual lines within the group and

their relative strength is supplemented by a number of models. Two extreme models are Elsasser model, in which equally spaced lines of equal intensity are considered and statistical model, in which the spectral lines are assumed to have random spacing and/or intensity. A typical spectral line arrangement for these models is shown in Figure 3.

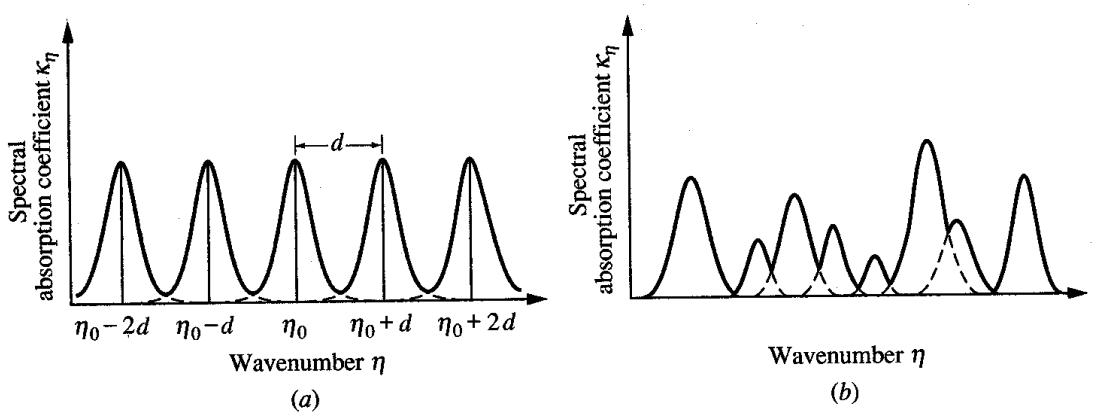

Figure 3. Typical Spectral Line Arrangements for (a) Elsasser and (b) Statistical Model [1]

In statistical model it is assumed that the spectral lines are not equally spaced but, rather, are randomly distributed across the narrow band. A statistical analysis can be carried out in two different ways. In the uniform statistical model the line intensity is assumed to be constant, leading to

$$\bar{\varepsilon}_\eta = 1 - \exp(\frac{W}{d}) \qquad (2.5)$$

where: $\bar{\varepsilon}_\eta$ -spectrally averaged emissivity

W -equivalent line width

d -spacing between spectral lines

In general statistical model, the statistical model has also been evaluated for exponentially decaying line intensities, resulting in

$$\bar{\varepsilon}_\eta = 1 - \exp\left(-\frac{(S/d)X}{\sqrt{1+\frac{SX}{\pi b_L}}}\right) = 1 - \exp\left(\frac{-\tau}{\sqrt{1+\frac{\tau}{\beta}}}\right) \qquad (2.6)$$

where: $\bar{\varepsilon}_\eta$ -spectrally averaged emissivity

S -line-integrated absorption coefficient

d -spacing between spectral lines

X -optical path length

b_L -line half width

-line overlap parameter

-narrow band optical thickness

The results from statistical model is summarized in Figure 4 and Table 1 in [1] as

	Weak line $x \ll 1$	Strong line $x \gg 1$	No overlap $\beta \ll 1$	All regimes
Single line, W	SX	$2\sqrt{SXb_L}$		$SXe^{-x}[I_0(x)+I_1(x)]$
$\frac{W}{d}$	τ	$2\sqrt{\frac{\tau\beta}{\pi}}$		$2\sqrt{\frac{\tau\beta}{\pi}\left(1-e^{-\pi\tau/4\beta}\right)}$
Elsasser Model, $\bar{\epsilon}_\eta$				
S = const	$1-e^{-\tau}$	$\operatorname{erf}\left(\sqrt{\tau\beta}\right)$	$\frac{W}{d}$	$\operatorname{erf}\left(\frac{\sqrt{\pi}}{2}\frac{W}{d}\right)$
d = const				
Statistical Model, $\bar{\epsilon}_\eta$				
S = const	$1-e^{-\tau}$	$1-\exp\left(-2\sqrt{\frac{\tau\beta}{\pi}}\right)$	$\frac{W}{d}$	$1-\exp\left(-\frac{W}{d}\right)$
d random				
Statistical Model, $\bar{\epsilon}_\eta$				
S exponential	$1-e^{-\tau}$	$1-\exp\left(-\sqrt{\tau\beta}\right)$	$\frac{\tau}{\sqrt{1+\tau/\beta}}$	$1-\exp\left(-\frac{\tau}{\sqrt{1+\tau/\beta}}\right)$
d random				
Definitions: $x=\frac{SX}{2\pi b_L}$, $\beta=\pi\frac{b_L}{d}$, $\tau=\frac{S}{d}X=2\beta x$				

Table 1. Summary of Effective Line Widths and Narrow Band Emissivities for Lorentz Lines [1]

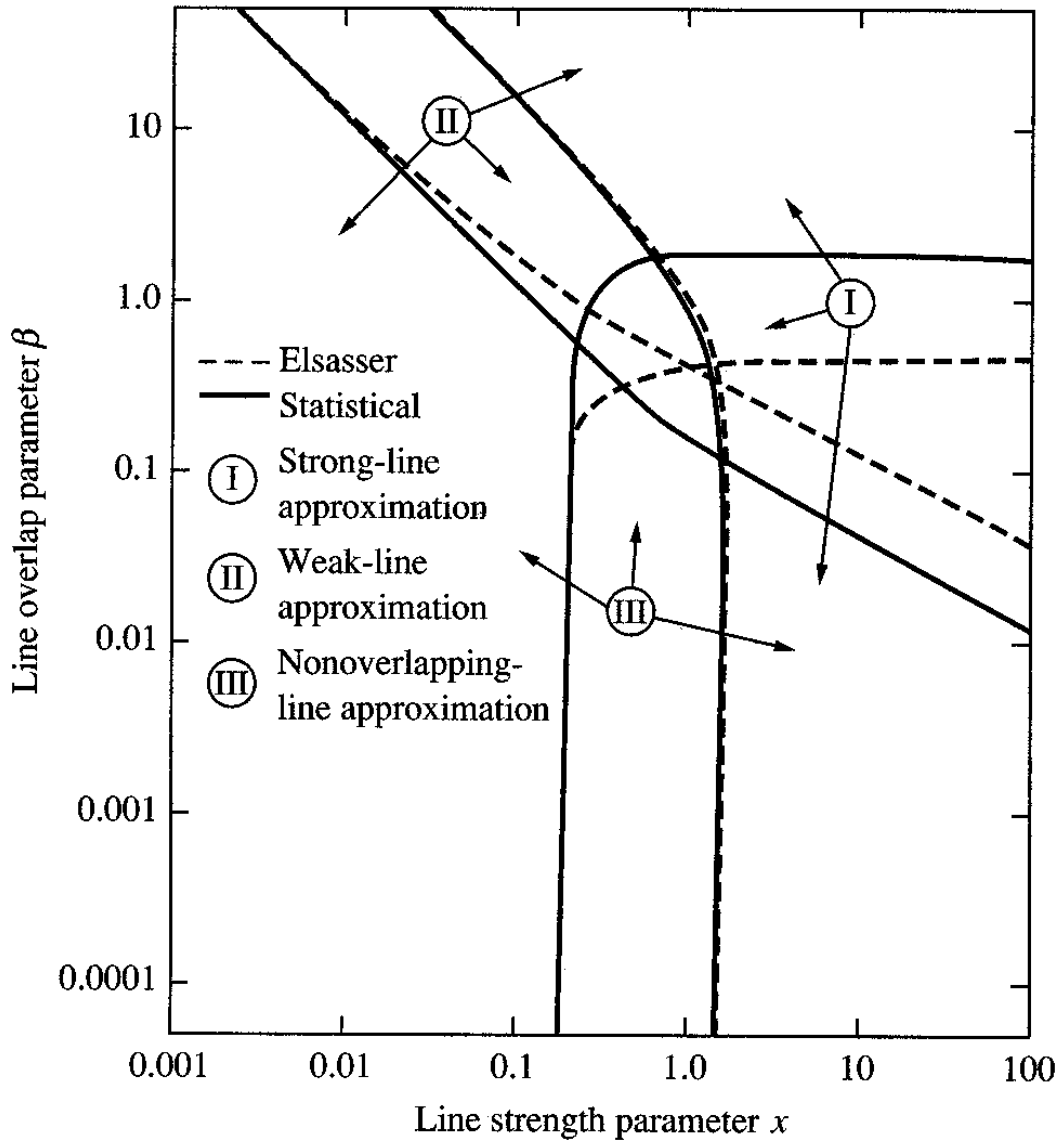

Figure 4. Regions of Validity for Elsasser and Statistical Band Model Regimes [1]

C. RADIATIVE TRANSPORT EQUATION (RTE)

In evaluating the radiative energy transport, it is required to know radiative properties, such as, emissivity,

absorptivity, and reflectivity in the case of surfaces, and absorption coefficient and scattering coefficient for the participating media such as gases. The law of conservation of energy is then applied to determine the energy field.

The general relationship that governs the behavior of radiative heat transfer in the presence of an absorbing, emitting medium is developed in [1]. RTE describes the radiative intensity field within the enclosure as a function of location, fixed by location vector r, direction, fixed by unit direction vector , and spectral variable, wavenumber . The net radiative heat flux crossing a surface element is obtained by adding up the contributions of radiative energy irradiating the surface from all possible directions and for all possible wavenumbers. Integrating the equation of transfer over all directions and wavenumbers leads to a conversation of radiative energy statement applied to an infinitesimal volume.

If the medium is participating, in that case any incident beam will be attenuated by absorption and scattering while radiative energy travels the medium, as shown in Figure 5.

The amount of absorption is directly proportional to the magnitude of the incident energy as well as the distance the beam travels through the medium. Thus,

$$(dI_\eta)_{abs} = -\kappa_\eta I_\eta ds \qquad (2.7)$$

where the proportionality constant κ_η is linear absorption coefficient. The negative sign is used to mean a decreasing intensity.

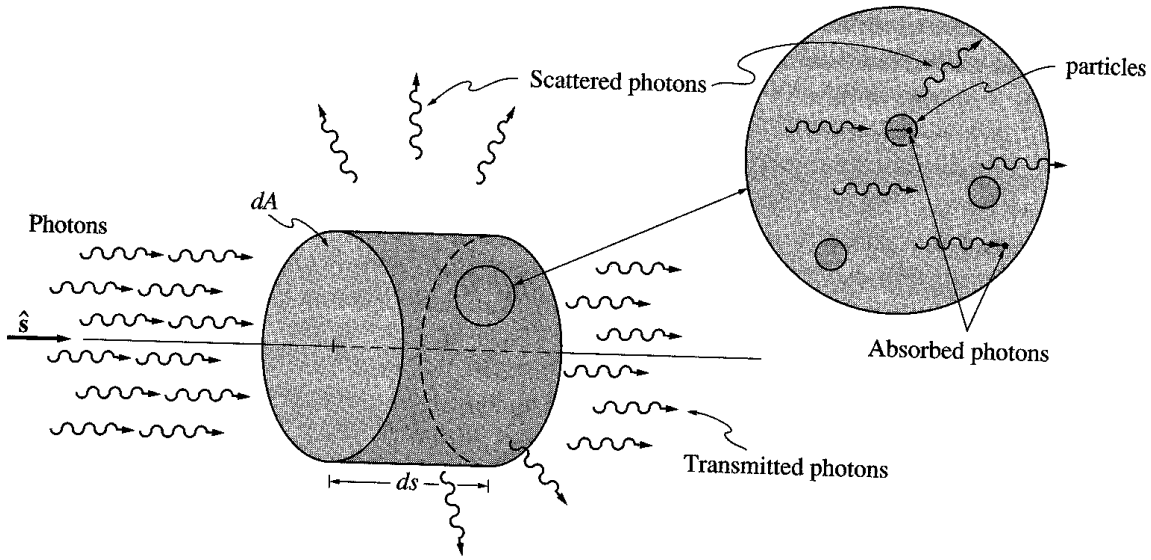

Figure 5. Attenuation of Radiative Intensity by Absorption and Scattering [1]

Attenuation by scattering or out-scattering is very similar to absorption, i.e., a part of the incoming intensity is removed from the direction of propagation, $\hat{s}$. It is different from absorption. Because absorbed energy is converted into internal energy, but scattered energy is simply redirected and appears as augmentation along another direction. Thus,

$$(dI_\eta)_{sca} = -\sigma_{s\eta} I_\eta ds \tag{2.8}$$

where the proportionality constant σ_{sn} is the linear scattering coefficient for scattering from the pencil of rays under consideration into all other directions.

A light beam traveling through a participating medium in the direction of $\hat{s}$ loses energy by absorption and scattering away from the direction of travel. But, it also gains energy by emission and by scattering from other directions into the direction $\hat{s}$.

The rate of emission from a volume element is proportional to the magnitude of the volume. The emitted intensity along any path is proportional to the length of the path and the local energy content in the medium. At thermodynamic equilibrium, the intensity everywhere must be equal to the blackbody intensity.

$$(dI_\eta)_{em} = \kappa_\eta I_{b\eta} ds \tag{2.9}$$

Augmentation due to in-scattering has contributions from all directions, and it is calculated by integration over all solid angles. The energy flux coming from all directions and scattered into the direction $\hat{s}$ is given in [1] as

$$(dI_\eta)_{sca} = ds \frac{\sigma_{s\eta}}{4\pi} \int_{4\pi} I_\eta(\hat{s}_i) \Phi_\eta(\hat{s}_i, \hat{s}) d\Omega \tag{2.10}$$

An energy balance from equations (2.7), (2.8), (2.9), and (2.10) results to RTE in [1] as

$$I_\eta(s+ds, \hat{s}, t+dt) - I_\eta(s, \hat{s}, t) = \kappa_\eta I_{b\eta}(s,t) ds - \kappa_\eta I_\eta(s, \hat{s}, t) ds - \sigma_{s\eta} I_\eta(s, \hat{s}, t) ds$$
$$+ \frac{\sigma_{s\eta}}{4\pi} \int_{4\pi} I_\eta(\hat{s}_i) \Phi_\eta(\hat{s}_i, \hat{s}) d\Omega_i ds \tag{2.11}$$

D. THE METHOD OF DISCRETE ORDINATES (S_N-APPROXIMATION)

The Discrete Ordinance Method (DOM) is a tool to transform the equation of transfer into a set of simultaneous partial differential equations. DOM is based on a discrete representation of the directional variation of the radiative intensity. A solution to the transport problem is found by solving the equation of transfer for a set of discrete directions spanning the total solid angle range of 4π. The discrete ordinates method is simply a finite differencing of the directional dependence of the equation of transfer. Integrals over solid angle are approximated by numerical quadrature.

The general equation of transfer for an absorbing, emitting, and anisotropically scattering medium is

$$\frac{dI}{ds} = \hat{s} \cdot \nabla I(r,\hat{s}) = \kappa(r) I_b(r) - \beta(r) I(r,\hat{s}) + \frac{\sigma_s(r)}{4\pi} \int_{4\pi} I(r,\hat{s}') \Phi(r,\hat{s}',\hat{s}) d\Omega' \quad (2.7)$$

Equation (2.7) is valid for a gray medium or, on a spectral basis, for a nongray medium, and is subject to the boundary condition

$$I(r_w,\hat{s}) = \varepsilon(r_w) I_b(r_w) + \frac{\rho(r_w)}{\pi} \int_{\hat{n}\cdot\hat{s}<0} I(r_w,\hat{s}) |\hat{n}\cdot\hat{s}| d\Omega' \quad (2.8)$$

where the enclosure is considered as opaque, diffusely emitting and reflecting wall.

In the discrete ordinates method, equation (2.7) is solved for a set of n different directions $\hat{s}_i$, i=1,2,Ö,n, and the integrals over direction are replaced by numerical quadratures, that is,

$$\int_{4\pi} f(\hat{s})d\Omega \cong \sum_{i=1}^{n} w_i f(\hat{s}_i) \qquad (2.9)$$

where, w_i is the quadrature weights associated with the directions s_i.

And, equation (2.7) becomes,

$$\hat{s}_i \cdot \nabla I(r,\hat{s}_i) = \kappa(r) I_b(r) - \beta(r) I(r,\hat{s}_i) + \frac{\sigma_s(r)}{4\pi} \sum_{j=1}^{n} w_j I(r,\hat{s}_j) \Phi(r,\hat{s}_i,\hat{s}_j), \qquad (2.10)$$

where, j=1,2,Ö,n, subject to boundary conditions

$$I(r_w,\hat{s}_i) = \varepsilon(r_w) I_b(r_w) + \frac{\rho(r_w)}{\pi} \sum_{\hat{n}\cdot\hat{s}_{j<0}} w_j I(r_w,\hat{s}_j) \left|\hat{n}\cdot\hat{s}_j\right| \qquad (2.11)$$

After determining the intensities, the radiative heat flux inside the medium or at a surface may be found as

$$q(r) = \int_{4\pi} I(r,\hat{s})\hat{s}d\Omega \cong \sum_{i=1}^{n} w_i I_i(r)\hat{s}_i \qquad (2.12)$$

In Table 3.2, the direction cosines of s_i and corresponding weights for S_4-approximation is shown. The direction cosines of s_i are

$$\hat{s}_i = (\hat{s}_i \cdot \hat{i})\hat{i} + (\hat{s}_i \cdot \hat{j})\hat{j} + (\hat{s}_i \cdot \hat{k})\hat{k} = \xi_i \hat{i} + \eta_i \hat{j} + \mu_i \hat{k} \qquad (2.13)$$

Only positive direction cosines are given in Table 3.2, covering one eight of the total range of solid angles 4 . To cover the entire 4 any or all of the values of ξ_i, η_i, and μ_i may be positive or negative.

Only positive direction cosines are given in Table 2, covering one eight of the total range of solid angles 4 .

To cover the entire 4 any or all of the values of ξ_i, η_i, and μ_i may be positive or negative.

Order of Approximation	Ordinates			Weights
	ξ	η	μ	w
S_4	0.2958759	0.2958759	0.9082483	0.5235987
	0.2958759	0.9082483	0.2958759	0.5235987
	0.9082483	0.2958759	0.2958759	0.5235987

Table 2. Discrete Ordinates for the S_4 Approximation [1]

THIS PAGE INTENTIONALLY LEFT BLANK

IV. NUMERICAL TOOLS

A. NUMERICAL SOLUTION STRATEGY

There are mainly three numerical tools used in this study.

First tool is TEP, which is used to calculate the thermodynamic chemical equilibrium properties of gas mixtures resulting from the combustion of various fuels and oxidants.

The second one is RADCAL, which is a numerical fire-modeling program which provides detailed gas spectral radiation data.

The third one is CFDACE, which is a set of computer programs for multi-physics computational analysis.

The numerical solution strategy flowchart is shown in Figure 6.

Figure 6. Numerical Solution Strategy Flowchart

B. TEP (THERMO-CHEMICAL EQUILIBRIUM PROGRAM)

TEP is used to calculate the thermodynamic chemical equilibrium properties of gas mixtures for a variety of different applications. Both thermodynamic data and ingredient libraries are included with TEP. The

applications that are included in the TEP program are Rocket Application, Gas Properties, Shock Application, Scramjet Application, Isentropic Path, and Detonation Application.

The application that is used is rocket problem. The rocket problem calculates the "theoretical", or maximum attainable performance, of a rocket thrust chamber. The calculations are based on the following assumptions:

- One-dimensional form of the continuity, energy, and momentum equations
- Zero velocity (stagnation) in the combustion chamber
- Complete combustion
- Adiabatic combustion
- Isentropic expansion
- Homogeneous mixing
- Ideal gas law
- Zero temperature and velocity lags between condensed and gaseous species

For equilibrium performance, composition is assumed to reach equilibrium immediately during expansion. For frozen performance, composition is assumed to remain fixed at the initial (stagnation) combustion composition during expansion.

Rocket performance is obtained by first determining stagnation combustion properties in the rocket chamber based on input of both enthalpy and pressure (H, P) or

temperature and pressure (T, P). Next, conditions at the nozzle throat are determined. The procedure used here is to find the pressure at which the flow velocity is equal to the sound speed. Iteration is required using entropy, pressure (S, P) point solutions, where the entropy is held fixed at the value calculated previously in the chamber. Once the throat conditions have been determined, solutions at input area ratios are obtained by iteration using (S, P) point solutions. For a given area ratio, A/A*, the entropy is held constant, and pressure is iterated until the product of density and velocity satisfies the continuity relation; i.e., a value equal to the throat density x throat velocity/ (A/A*).

There are two main inputs to the rocket application, thermochemistry and rocket operating conditions. In thermochemistry chemical reactants, thermochemical species data, and reactants mixture specification is defined. Under thermochemistry chemical reactants option, the ingredients that will be used as oxidizer and fuel are selected. And oxidizer to fuel ratio is entered. Under thermochemical species data option, the species that will be used in the application is selected between CHNO, CHO, HO, SRM, Master Thermo, and Air/Hydrogen file. The properties of these files are as follows:

CHNO Thermodynamic Data File contains 29 species screened for use in air/hydrocarbon combustion problems. This set of species is more than sufficient for most CHNO problems. The study was done by screening calculated results obtained using the master files. The calculations

were for air/acetylene and air/methane for a broad range of pressure, temperature, and equivalence ratio.

CHO Thermodynamic Data File contains 20 species screened for use in oxygen/hydrocarbon combustion problems. It has been obtained from the CHNO thermo data file by omitting species containing N.

HO Thermodynamic Data File contains 8 species screened for use in oxygen/hydrogen combustion problems. It has been obtained from the CHO thermo data file by omitting species containing C.

Solid Propellant Rocket Motor File contains the principal species that make up the exhaust of aluminized solid propellant rocket motors.

Master Thermodynamic Data File contains data for approximately 1000 chemical species. It can be edited to produce short files containing only those species important to specific problems. Several files of this type are also provided. Principal species of the following elements are contained in this master file: Al, Ar, B, Ba, Be, Br, C, Ca, Cl, Cr, Cs, Cu, D, F, Fe, H, He, Hg, I, K, Li, Mg, N, Na, Nb, Ne, Ni, O, P, Pb, S, Si, Sr, Ta, Ti, V, Xe, Zn, and Zr. The electron and positive or negative ion forms for a limited number of species are also provided. Please note that the master file is intended as a library, and not for general problem solving use. The master file will often yield too many species for problem solving, especially when a reactant contains the element carbon.

Air/Hydrogen File is intended for use in Air/Hydrogen combustion problems, such as occur in flame propagation and shock tube studies.

Under rocket operating conditions option, chamber pressure in atmosphere, chamber temperature in Kelvin, subsonic area, supersonic area, and pressure ratios are entered.

Table 3 shows the input and output data for TEP program.

INPUT DATA	OUTPUT DATA
Gas temperature, gas pressure, oxidizer to fuel ratio, subsonic and supersonic area ratios	Chamber and exit pressure, participating gas temperature, density, molecular weight, sonic velocity, prandtl number, mixture speciesí mole fractions, mass fractions.

Table 3. Input and Output Data for TEP Program

C. RADCAL

RADCAL is a narrow band numerical model developed at NIST for radiation calculations in a combustion environment. RADCAL is a numerical program, which predicts the radiant intensity leaving a nonisothermal volume containing nonuniform levels of carbon dioxide, water vapor, methane, carbon monoxide, nitrogen, oxygen, and soot. The absorption coefficient of the combined gases is

calculated from a narrow-band model and a combination of tabulated spectral properties and theoretical approximations to the vibrational-rotational molecular bands.

Table 4 summarizes the species and their molecular bands currently in RADCAL.

Species	Band
CO_2	2.0 μm
CO_2	2.7 μm
CO_2	4.3 μm
CO_2	10.0 μm
CO_2	15.0 μm
H_2O	1.38 μm
H_2O	1.88 μm
H_2O	2.7 μm
H_2O	6.3 μm
H_2O	20-200 μm
CO	4.6 μm
CH_4	2.4 μm
CH_4	3.3 μm
CH_4	7.7 μm
soot	0.4-2000 μm

Table 4. Molecular Bands Included in RADCAL [3]

The numerical code consists of a short main program which reads the temperature and concentration information from the data file, RC DAT. SUBROUTINE RADCAL is called from the main program to perform all the calculations. RCOUT DAT is the file that contains the outputs. Figure 7 is a diagram of the structure of the program.

RADCAL relies upon the four subroutines to compute the narrow-band parameters for the carbon dioxide

(SUBROUTINE CO_2), water vapor (SUBROUTINE H_2O), carbon monoxide (SUBROUTINE CO), and methane (SUBROUTINE FUEL). Two large block data files (BLOCK DATA BD1 and BLOCK DATA BD2) contain the absorption coefficient of water vapor as a function of temperature and wave number. A third data file, BLOCK DATA BD3, contains similar information for the 15 m band CO_2, and the 3.3 and 7.4 m bands of CH_4.

When the path contains only one element three different absorption coefficients are calculated the Planck-mean, the incident-mean, and the effective absorption coefficient.

In the first line of the input data file, RC DAT, the number of elements into which the path is divided, NPT, is written. The second line lists the size of the first element in meters, DD (1), its temperature in Kelvin, T (1), and the partial pressures in kilopascals of carbon dioxide, P (1,1), water vapor, P (1,2), methane, P (1,3), carbon monoxide, P (1,4), oxygen, P (1,5),and nitrogen, P (1,6). The last entry on the second line is the volume fraction of soot in the first element, W (1). The third line contains the size, temperature, species partial pressure, and soot volume fraction for the second element.

Similar data is entered for the remainder of the NPT elements. Following this information is a line containing the wall temperature in Kelvin, TWALL, and the minimum and maximum wavenumbers in cm^{-1}, OMMIN and OMMAX. The program terminates when it reads zero for the value of NPT.

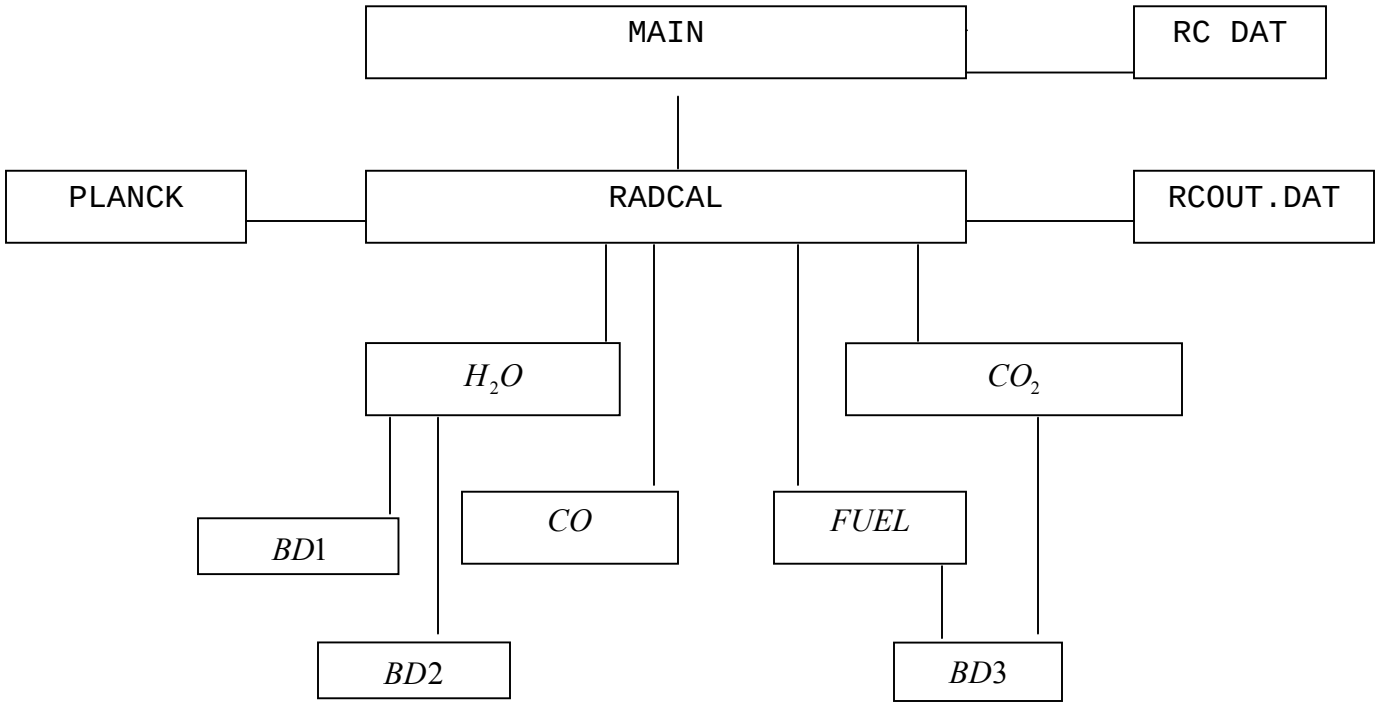

Figure 7. Structure of Radiation Calculation Program RADCAL [3]

The results of the calculations are found in the output file, RCOUT DAT. The input conditions are summarized in tabular form, followed by the total directional radiated energy flux emanating outward from element one, Q. The spectral intensity, QW (K) and the transmittance, TTAU (K), are listed for each wavelength, AMBDA (K). The program also calculates the effective-mean absorption coefficient, AMEAN, the Planck-mean absorption coefficient, APO, and the wall-incident-mean absorption coefficient, AIWALL.

Table 5 shows the input and output data for RADCAL program.

INPUT DATA	OUTPUT DATA
The number of elements, size of the elements, temperature of the elements, partial pressures of carbon dioxide, water vapor, methane, carbon monoxide, oxygen, and nitrogen, volume fraction of soot, wall temperature, minimum and maximum wavenumbers.	Total directional radiated energy flux, the spectral intensity and the transmittance for each wavelength, the effective-mean absorption coefficient, the Planck-mean absorption coefficient, and the wall-incident-mean absorption coefficient.

Table 5. Input and Output Data for RADCAL Program

D. CFD-ACE+

CFD-ACE+ is a set of computer programs for multi-physics computational analysis released by CFD Research Corporation. The programs provide an integrated geometry and grid generation module, a graphical user interface for preparation of the model, a computational solver for performing the simulation, and an interactive visualization program for examination and analysis of simulation results. CFD-ACE+ package include the following applications:

- CFD-GEOM Interactive 3D Geometry Modeling and Mesh Generation (Structured, Unstructured, and Mixed-Element Meshes)
- CFD-GUI Solver Setup Interface
- CFD-ACE (U) General Purpose Multi-Disciplinary Physics Solver
- CFD-VIEW Interactive 3D Graphics, Animation & Flow Visualization Software

Figure 8 shows the applications that are included in CFD-ACE + package.

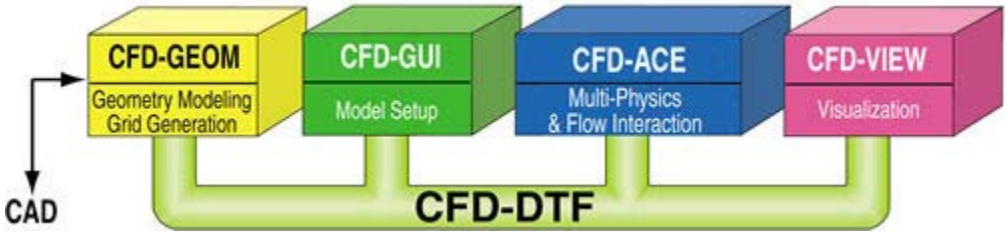

Figure 8. CFD ACE+ Package [9]

1. CFD-GEOM

CFD-GEOM is an interactive CAD type geometry creation and fast grid generation (structured, unstructured and hybrid grids) program for Computational Fluid Dynamics (CFD). The geometry module allows the user to interactively define the geometry or modify the geometry read through the Plot3D data format.

It serves as the front-end of CFDRC's solver packages and can be used with any other CFD/FEA/CAE program. With

interfaces to read geometry data created in almost any major commercial CAD program, it integrates CFDRC's CFD packages into the existing CAE environment.

CFD-GEOM uses efficient data structures providing flexible inter-domain connectivity, part merging, and easy manipulation of all entities (geometry, topology, structured, unstructured meshes) with rapid database updating. Entity manipulations include translation, rotation, scaling, copying, (un)deleting, blanking, labeling, and model merging/extracting. Topological entities include:

- Edges - composed of single or multiple curves and/or lines.
- Faces - comprising single or multiple edge sets or single surfaces, possibly projected to surfaces.
- Blocks - consisting of single or multiple volumes or face sets. Arbitrary orientation between adjacent blocks is allowed, or a consistent multi-block orientation can be requested automatically (hence no need to pre-plan individual IJK node directions).
- Composition of edges, faces and blocks.
- Edge-linking - any number of edges can be linked to a smaller number of master edges for mesh density and/or distribution, requiring minimum effort to modify mesh characteristics.
- Boundary Conditions- the location and type of boundary condition for the flow solvers can be prescribed in

CFD-GEOM, providing automatic updating during mesh refinement or geometry change.

2. CFD-ACE (U)

CFD-ACE is an unstructured, polyhedral cell flow solver. It is also integrated with a wide variety of other physics modules making it the core of a multi-disciplinary analysis environment. CFD-ACE employs a cell-centered control volume solution approach. This approach implies that the discrete equations are formulated by evaluating and integrating the fluxes across the faces that surround each control volume.

CFD-ACE provides an integrated geometry and grid generation module.

3. CFD-VIEW

CFD-VIEW is a 3-D post processor included in CFD-ACE+, which reduces the large volume of data generated by CFD-ACE to useful information. CFD-VIEW is an interactive graphics program for post-processing numerical results from CFD and other analysis software. It provides an easy-to-use and interactive environment, with many graphics tools to visualize the flow physics, as well as the ability to extract data relevant to engineering design.

V. CODE CALIBRATION AND BENCHMARKING

A. NUMERICAL TOOL CALIBRATION

Geometry of the model is created by the pre-processor CFD-GEOM. Creating the structured grid is done by grid generation module in a bottom-up approach in labeling geometry elements as edges, faces, and blocks. In order to achieve the best results, the calibration is done when the participating medium is not present. This helps to compare the results with the hand calculations.

The following parameters are considered when calibrating the model:

- The edge parameters
- The number of iterations
- The error in the wall convection

The model is created by 25, 50, 100, and 200 points consecutively. The edge parameters dictate how many grid points are placed on the edge and how these grid points are distributed. The power law is used as a grid point distribution method. The power law distribution is defined by

$$u(n) = \left(\frac{n-1}{npts-1} \right)^{x} \qquad (5.1)$$

where: $u(n)$ -location of grid point on the interval [0Ö1]

n -grid points index on the interval [1Önpts]

npts -the number of grid points

x -user-specified power

The power law is usually close to one which corresponds to a uniform distribution. For non-unity powers, the forward, backward, and symmetry options indicate how the power law grid distribution is applied.

The geometry is created with 25, 50, 100 and 200 points, while the power law grid scaling scheme is varied between 1.3, 1.5 and 2. Convergence criteria were varied from 1e-04 to 1e-10. Figure 9 discusses the results for convergence criteria of 1e-08.

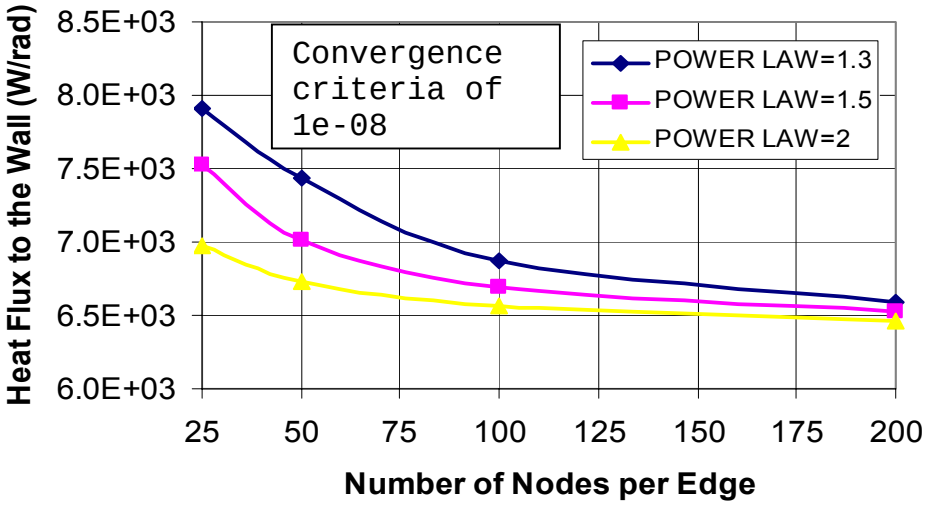

Figure 9. Total Heat Flux Values for Various Power Law Grid Scaling Schemes

As seen in the figure, the heat flux value for 100 points with power law of 2 converges more rapidly than the

others and a 100 point grid was found to be a good trade-off between accuracy and computational time.

B. TRASPARENT MEDIUM CASE

Numerical results are compared with the analysis of radiative heat transfer within enclosures without participating medium. Figure 10 defines the surfaces and the emissivities corresponding to these surfaces.

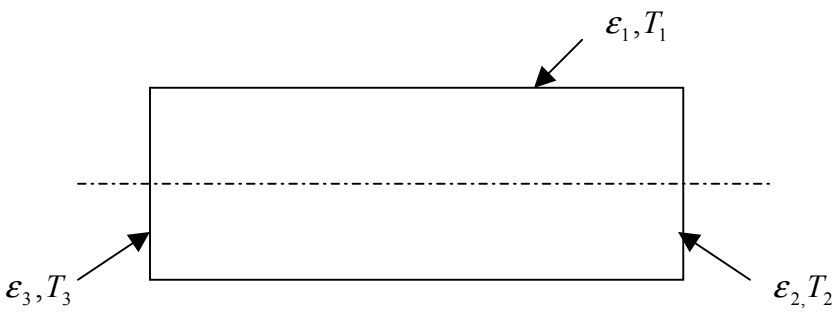

Figure 10. Two Dimensional Cylinder

Radiative exchange between black surfaces is calculated from the following expression in [1] as

$$q_i = \sum_{j=1}^{N} F_{i-j}(E_{bi} - E_{bj}) \qquad (5.2)$$

where:

N -number of surfaces

F_{i-j} -view factor from surface i to j

E_{bi} -blackbody emissive power of surface i

The equation 5.2 becomes

$$q_1 = F_{1-1}(E_{b1} - E_{b1}) + F_{1-2}(E_{b1} - E_{b2}) + F_{1-3}(E_{b1} - E_{b3}) \quad (5.3)$$

where the view factors can be calculated from view factor catalogue. [2]

Table 6 shows the comparison of the hand calculations and CFD-A software results for wall temperature of 400 F and gas temperature of 3500 K between black surfaces.

	Hand Calculation	Numerical Results	Relative Error (%)
Radiation to the Wall (watts/rad)	-2882.46	-2795	3.02

Table 6. Relative Error in Radiative Exchange Between Black Surfaces

Similarly, radiation exchange between gray and diffuse surfaces can be calculated from the following expression [1]

$$\frac{q_i}{\varepsilon_i} - \sum_{j=1}^{N}(\frac{1}{\varepsilon_j} - 1)F_{i-j}q_j = \sum_{j=1}^{N} F_{i-j}(E_{bi} - E_{bj}) \quad (5.4)$$

The equation (5.4) becomes

$$\frac{q_1}{\varepsilon_1} - (\frac{1}{\varepsilon_1} - 1)F_{1-1}q_1 = F_{1-1}(E_{b1} - E_{b1}) + F_{1-2}(E_{b1} - E_{b2}) + F_{1-3}(E_{b1} - E_{b3}) \quad (5.5)$$

Table 7 shows the comparison of the hand calculations and CFD-ACE software results for wall temperature of 400 F and gas temperature of 3500 K between gray surfaces.

The relative error is due to the fact that in hand calculations the outlet is assumed to be isothermal, which is not the case for real cases.

	Hand Calculation	Numerical Results	Relative Error (%)
Radiation to the Wall (watts/rad)	-2512.24	-2369	5.701

Table 7. Relative Error in Radiative Exchange Between Gray Surfaces

C. GRAY GAS CASE

A literature search shows that, although there is an extensive search for the gray gas approximation, the pressure and temperature values are limited to the temperatures and pressure values lower than that of interest in this study.[2,6,7,8]. Next, CFD-ACE results are compared with hand calculations for different optical thickness values for parallel plate and round tube cases with participating medium. Parallel plate and round tube cases are considered consecutively.

1. Parallel Plate

In parallel plate case, a gray, nonscattering medium is contained between two parallel gray plates. The medium is isothermal at temperature T_g, with constant absorption coefficient κ. The two plates are isothermal at temperature T_w, have the same gray-diffuse emissivity , and are spaced a distance D apart as shown in Figure 11.

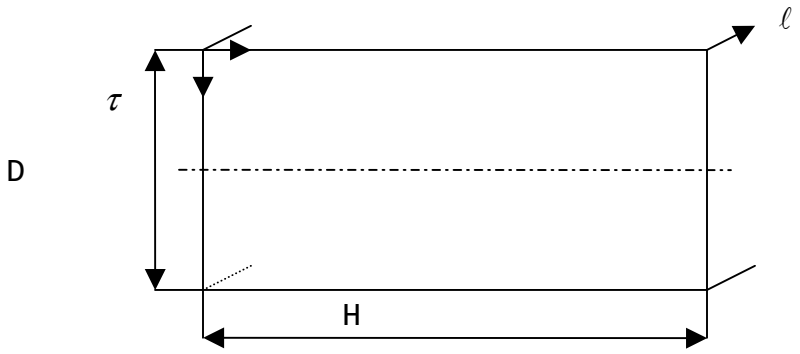

Figure 11. Coordinate System and Dimensions for the Parallel Plate

Heat flux at for the specified conditions is given in [1] as

$$q(\tau) = \sigma(T_w{}^4 - T_g{}^4)\frac{2[E_3(\tau) - E_3(\tau_L - \tau)]}{1 + (\frac{1}{\varepsilon} - 1)[1 - 2E_3(\tau_L)]} \qquad (5.6)$$

At the wall τ is equal to zero. So, the equation becomes

$$q(\tau = 0) = \sigma(T_w{}^4 - T_g{}^4)\frac{2[E_3(0) - E_3(\tau_L)]}{1 + (\frac{1}{\varepsilon} - 1)[1 - 2E_3(\tau_L)]} \qquad (5.7)$$

and

$$q(\tau = 0) = \sigma(T_w{}^4 - T_g{}^4)\frac{[1 - E_3(\tau_L)]}{1 + (\frac{1}{\varepsilon} - 1)[1 - 2E_3(\tau_L)]} \qquad (5.8)$$

Equation 5.8 is valid for all the optical thickness values other than zero and infinity. For optically thick and optically thin cases, two different solutions are necessary.

In optically thick case τ_L goes to infinity and Equation (5.8) becomes

$$q = \varepsilon\sigma(T_w{}^4 - T_g{}^4) \qquad (5.9)$$

In the optically thin situation the following result for total heat loss is used for any isothermal volume without self absorption in [1]

$$Q = 4\kappa n^2 \sigma T_g{}^4 V \qquad (5.10)$$

Multiplying and dividing this equation with 2R and writing the heat flux gives

$$q = \frac{Q}{A_s} = \frac{4\tau_L n^2 \sigma T_g{}^4 V / 2R}{(2H\ell + 2D\ell + 2HD)} = \frac{2\tau_L n^2 \sigma T_g{}^4}{1 + \frac{D}{H} + \frac{D}{\ell}} \qquad (5.11)$$

where, V is total volume and A_S is the surface area.

Assumption of ℓ is greater than D and H is a very good one and equation (5.11) becomes

$$q = \frac{Q}{A_s} = \frac{4\tau_L n^2 \sigma T_g{}^4 V / 2R}{(2H\ell + 2D\ell + 2HD)} = \frac{2\tau_L n^2 \sigma T_g{}^4}{1 + \frac{D}{H}} \qquad (5.12)$$

Since the case is optically thick, taking two values for τ_L is good enough, such as zero and one. The other unknown is D/H ratio and for this values, zero and one and a half is chosen. Zero corresponds to a very long parallel plate, which makes H equal to infinity, but it causes to deteriorate the true geometry. On the other hand, one and a half corresponds to the real geometry. Figure 12 and 13 compare the theoretical radiation to the wall values with CFD-ACE results for various optical thicknesses, for optically thick and optically thin case in a parallel plate.

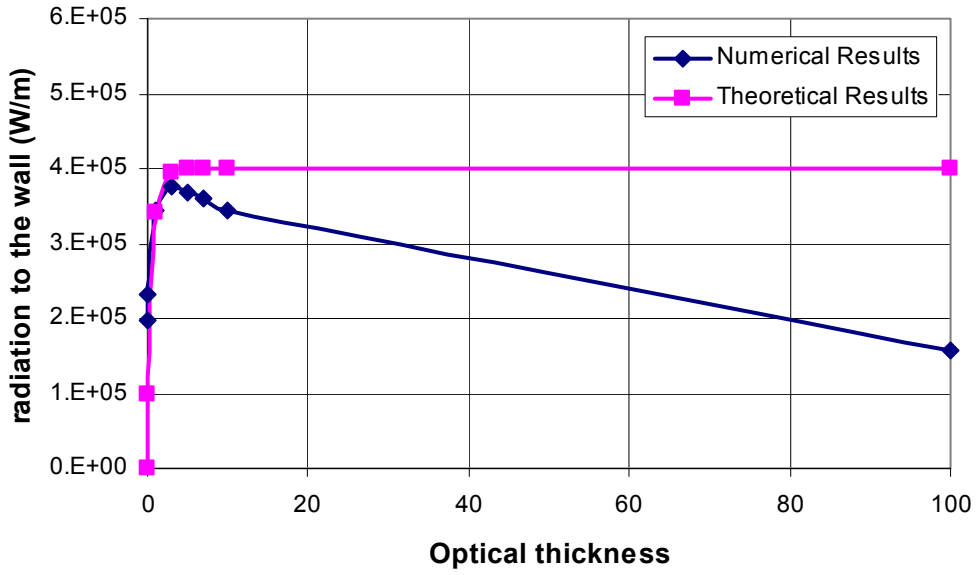

Figure 12. Comparison of Theoretical and Numerical Results for Parallel Plate

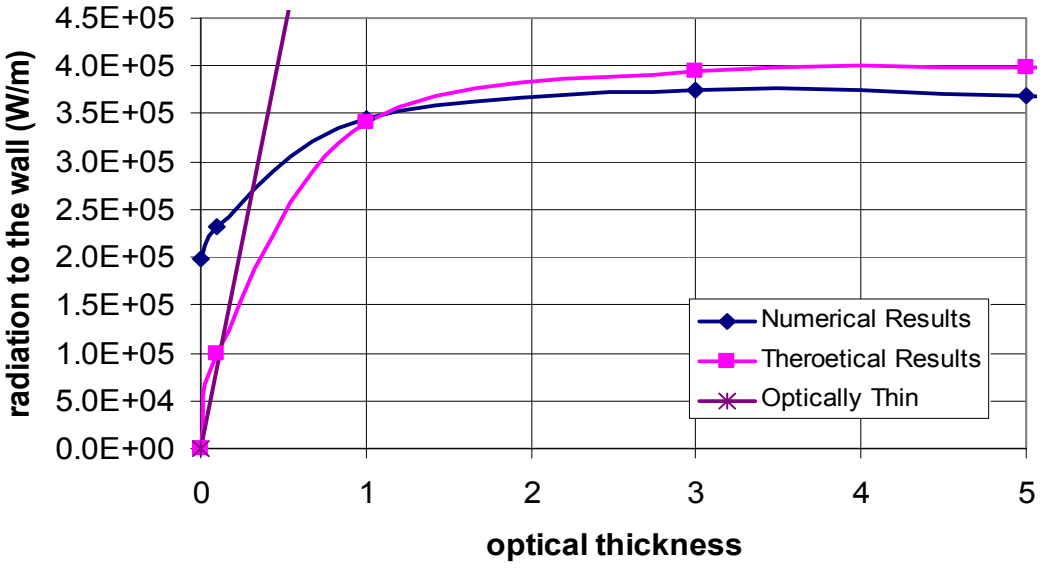

Figure 13. Comparison of Theoretical and Numerical Results for Parallel Plate (magnified)

2. Round Tube

In round tube case, a gray, nonscattering medium is contained between the walls of the cylinder. The medium is isothermal at temperature T_g, with constant absorption coefficient κ. The wall of the cylinder is isothermal at temperature T_w, have the gray-diffuse emissivity , and the radius is R as shown in Figure 14.

The nondimensional heat loss from a gray, nonscattering, isothermal cylinder is given in [1] as

$$\psi = \frac{q(\tau_R)}{n^2 \sigma T_g^{\ 4} - J_w} \tag{5.13}$$

where, J_w is the radiosity of the wall. Some representative results of equation (5.13) for $\tau=\tau_R$ have been tabulated in Table 8. [1]

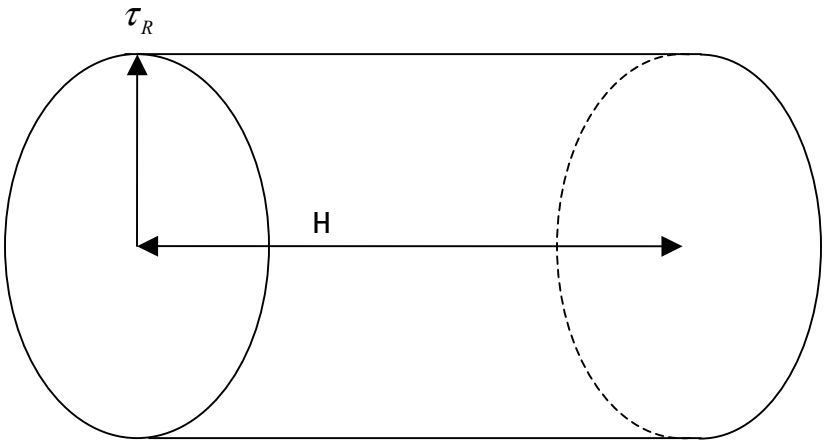

Figure 14. Coordinate System and Dimensions for the Round Tube

τ_R	ψ
0.1	0.1770
0.5	0.5960
1.0	0.8143
5.0	0.9923

Table 8. Nondimensional Heat Loss from a Gray, Nonscattering, Isothermal Cylinder [1]

Since the walls are not black, but are gray, diffuse emitters and reflectors, the heat flux to the wall is no longer πI_b, but must be replaced by the radiosity.

$$q(\tau_R) = \psi(n^2 \sigma T_g{}^4 - J_w) = (J_w - E_{bw}) \frac{\varepsilon_w}{1-\varepsilon_w} \tag{5.14}$$

Since the walls are not black, but are gray, diffuse emitters and reflectors, the heat flux to the wall is no longer πI_b, but must be replaced by the radiosity.

$$q(\tau_R) = \psi(n^2 \sigma T_g{}^4 - J_w) = (J_w - E_{bw}) \frac{\varepsilon_w}{1-\varepsilon_w} \tag{5.14}$$

So, the radiosity becomes

$$J_w = \frac{(\psi n^2 \sigma T_g{}^4) + (\frac{\varepsilon_w}{1-\varepsilon_w} \sigma T_w{}^4)}{\frac{\varepsilon_w}{1-\varepsilon_w} + \psi} \tag{5.15}$$

And the heat flux is

$$q(\tau_R) = \sigma\psi \left[(n^2 T_g{}^4) - \frac{(\psi n^2 T_g{}^4) + (\frac{\varepsilon_w}{1-\varepsilon_w} T_w{}^4)}{\frac{\varepsilon_w}{1-\varepsilon_w} + \psi} \right] \tag{5.16}$$

Equation 5.16 is valid for all the optical thickness values other than zero and infinity. For optically thick and optically thin cases, two different solutions are necessary.

In optically thick case ψ goes to one according to Table 8 and Equation (5.16) becomes

$$q(\tau_R) = \sigma\left[(n^2 T_g{}^4) - \frac{(n^2 T_g{}^4) + (\frac{\varepsilon_w}{1-\varepsilon_w} T_w{}^4)}{\frac{\varepsilon_w}{1-\varepsilon_w}}\right] \qquad (5.17)$$

In the optically thin situation the following result for total heat loss is used for any isothermal volume without self absorption in [1]

$$Q = 4\kappa n^2 \sigma T_g{}^4 V \qquad (5.18)$$

Multiplying and dividing this equation with R and writing the heat flux gives

$$q = \frac{Q}{A_s} = \frac{4\tau_R n^2 \sigma T_g{}^4 V / R}{(\pi R^2 + \pi R^2 + 2\pi RH)} = 2\tau_R n^2 \sigma T_g{}^4 (\frac{1}{\frac{R}{H}+1}) \qquad (5.11)$$

where, V is total volume of the cylinder and A_S is the surface area.

Since the case is optically thick, taking two values for τ_R is good enough, such as zero and one. The other unknown is R/H ratio and for these values, zero and one quarter is chosen. Zero corresponds to a very long cylinder, which makes H equal to infinity, but it causes to deteriorate the true geometry. On the other hand, one quarter corresponds to the real geometry. Figure 15 and 16 compares the theoretical radiation to the wall values with CFD-ACE results for various optical thicknesses, for optically thick and optically thin case in a round tube.

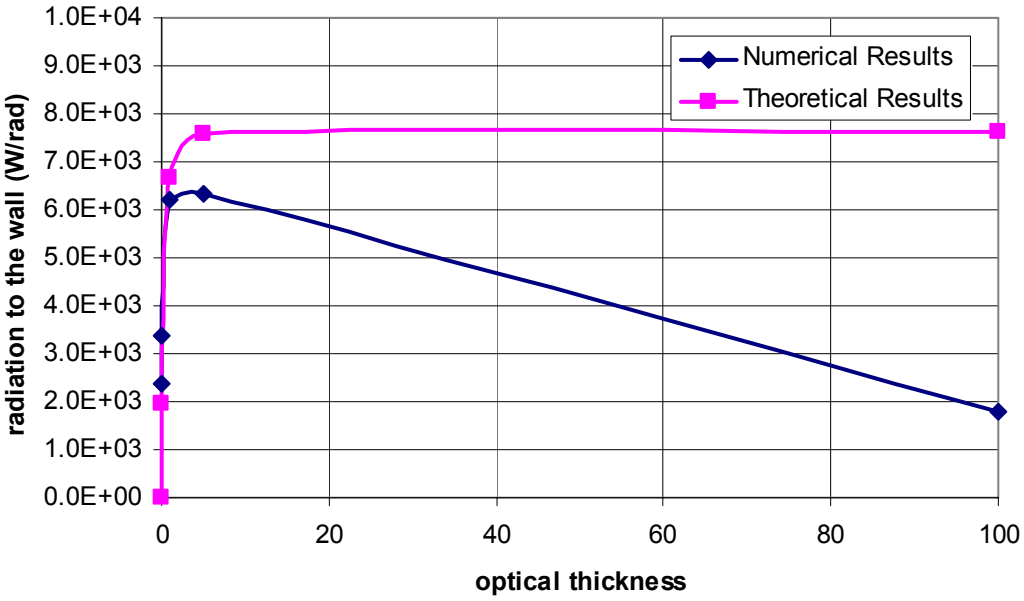

Figure 15. Comparison of Theoretical and Numerical Results for Round Tube

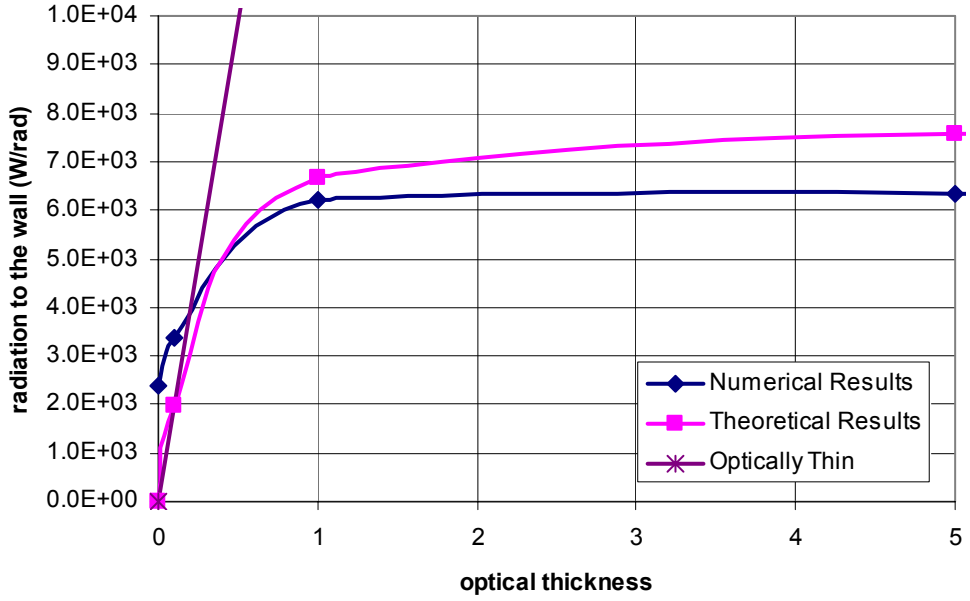

Figure 16. Comparison of Theoretical and Numerical Results for Round Tube (magnified)

It is obvious that, as the participating gas gets optically thick the results do not agree since, in reality, the gas is not isothermal across the chamber cross-section.

When the gas is optically thick, its absorption coefficient is large, so the typical absorption length scale is small. In other words, emission from the gas is reabsorbed over a very short distance. In such a scenario, the radiation on the wall comes from the region of gas close to the wall where the gas is at a lower temperature than the core temperature (due to the boundary layer nature of the temperature profile), and is hence a lower heat flux value.

An important point is to investigate if these hand calculations contain radiation to the wall according to the expressions used herein or not. So, in order to compare these results with each other, the value of radiation to the wall for gray walls, transparent medium from CFD-ACE, is not added to the hand calculation results. This is shown in Appendix A.

D. NON-GRAY GAS CASE

A literature search shows that only a limited number of non-gray cases have been treated in the past, and have been restricted to pure gases at temperatures and pressures lower than that of interest in this study [4,5]. The radiation heat flux in CO for 1000 ^{0}R gas temperature at 1 atmosphere pressure and 500 ^{0}R wall temperature with a parabolic initial velocity distribution is considered. The

parabolic velocity profile at the inlet is created by using the following expression and shown if Figure 17.

$$U = 2U_{ave}(1-\frac{y^2}{R^2}) \qquad (5.12)$$

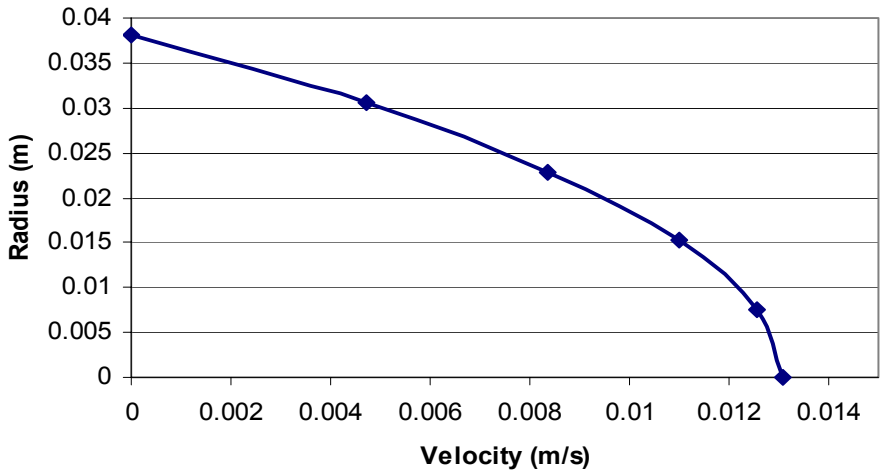

Figure 17. Parabolic Velocity Profile at the Inlet

Where, U_{ave} is found from the following expression.

$$U_{ave} = \frac{\mathrm{Re}^* \mu}{\rho * D} \qquad (5.13)$$

By using the fire prediction program RADCAL, the intensities and transmissivities are found based on the wavelength as shown below in Figure 18.

The numerical result and published result are compared in Figure 19 and compared with [4]. The published results and numerical results agree well.

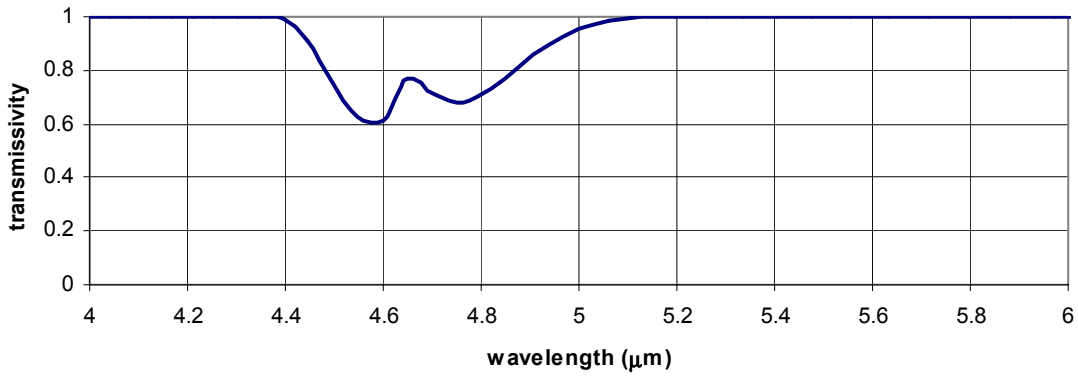

Figure 18. RADCAL Output for Transmissivity of Pure CO

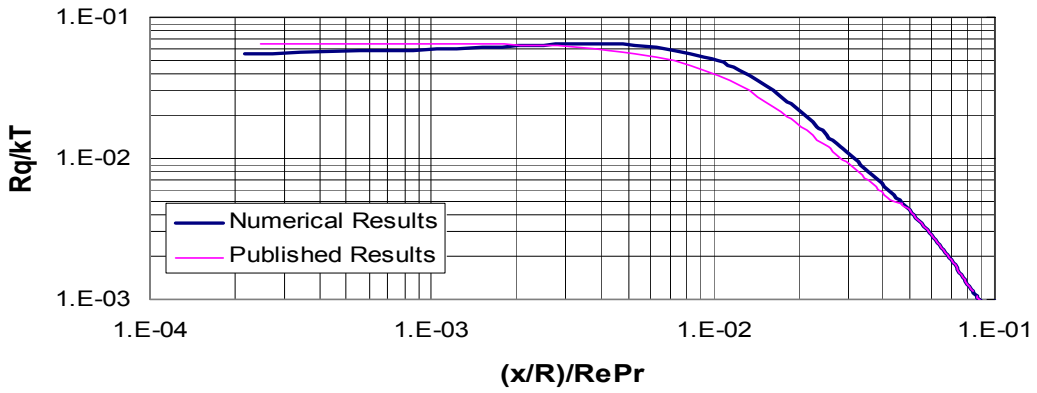

Figure 19. CFD Output for the Specified Conditions

VI. RESULTS AND DISCUSSIONS

The model problem being treated in this study contains several parameters, such as the gas optical thickness, the conduction to radiation parameter, the emissivity and temperature of the wall, the gas mixture constituents and its temperature, etc. Of these, only the parameters of primary importance were varied in a parametric study as described below so as to determine the role of the main contributing factors to the radiative heat loading of the duct wall.

The results presented here are obtained using a 100x100 grid. Further subdivision of the enclosure does not yield significantly more accurate results under the specified convergence criteria. Convergence is checked using a tolerance of 1e-10. The CPU time required to generate the results varied from 22 minutes to 107 minutes (per run) depending on the complexity of the case.

A. GRAY GAS CASE

Under the gray gas approximation, a parametric study was conducted by varying gas temperature, wall temperature, wall emissivity, and optical thickness. The role of the gas temperature for the gray gas approximation is shown in Figure 20 and 21. Figure 20 shows the convective and radiative heat fluxes to the wall versus the optical thickness for a low gas to wall temperature ratio and for a high gas to wall temperature ratio. It is evident that there is an optimal optical thickness at which the

radiative flux is a maximum, which can be seen clearly in Figure 20. As expected the radiative flux is higher on the black wall, and higher gas temperatures. In both figures, it is shown that, the radiative flux is a significant fraction of the total heat flux especially in the large gas-to-wall temp ratio case.

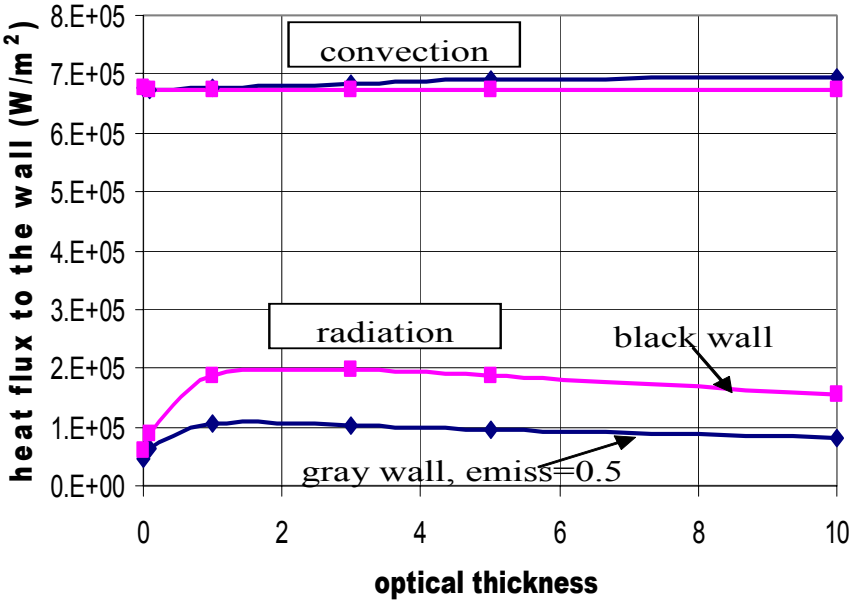

Figure 20. Convective and Radiative Heat Flux for 1500K Gas 800K Wall Temperature

The dependence on wall emissivity for the gray gas approximation is shown in Figure 22 and Figure 23. These figures show the relative contribution of the radiative heat flux versus the non-dimensional length along the duct for low gas to wall temperature and for high gas to wall temperature ratios, respectively. An optical thickness of 3

is used which is close to the optimal value as shown in the previous figures for maximum radiative flux. It is clear that the relative radiative contribution for the high gas temperature is almost twice that for the low temperature case.

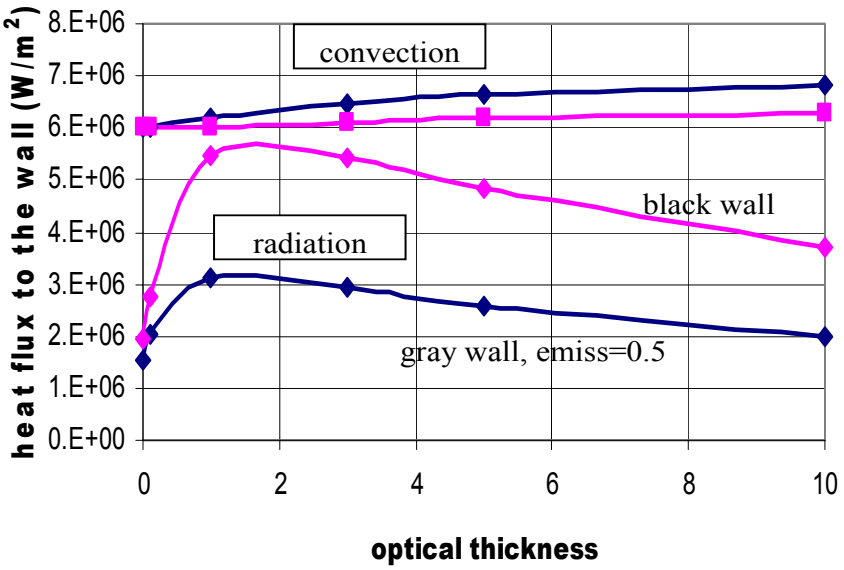

Figure 21. Convective and Radiative Heat Flux for 1500K Gas 800K Wall Temperature

Figures 24 and Figure 25 show the radiative heat flux versus the non-dimensional length along the duct for different wall temperatures at 3500 K gas temperature.

It is clear in Figure 25 that, the absolute heat flux values are nearly the same, although in Figure 24, the relative contribution is slightly higher for the hotter wall.

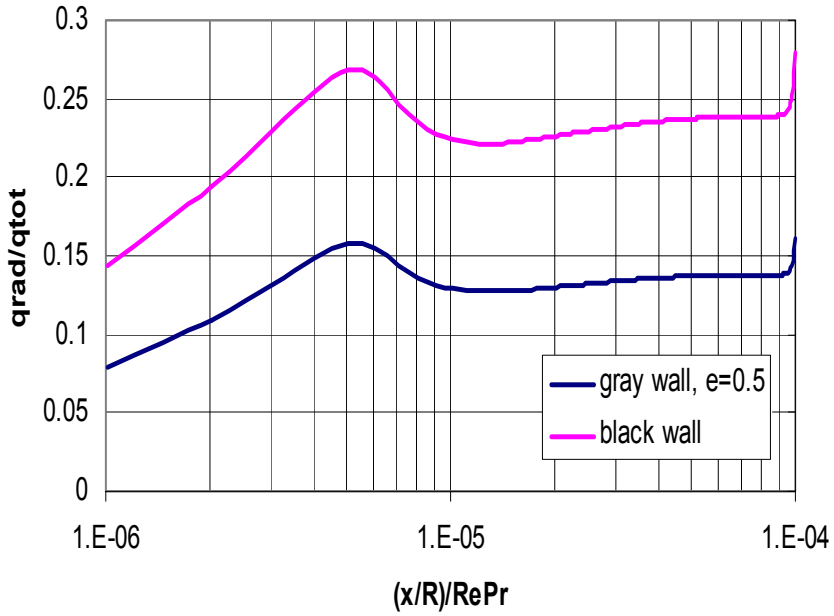

Figure 22. Relative Contribution of the Radiative Heat Flux in Different Wall Emissivities

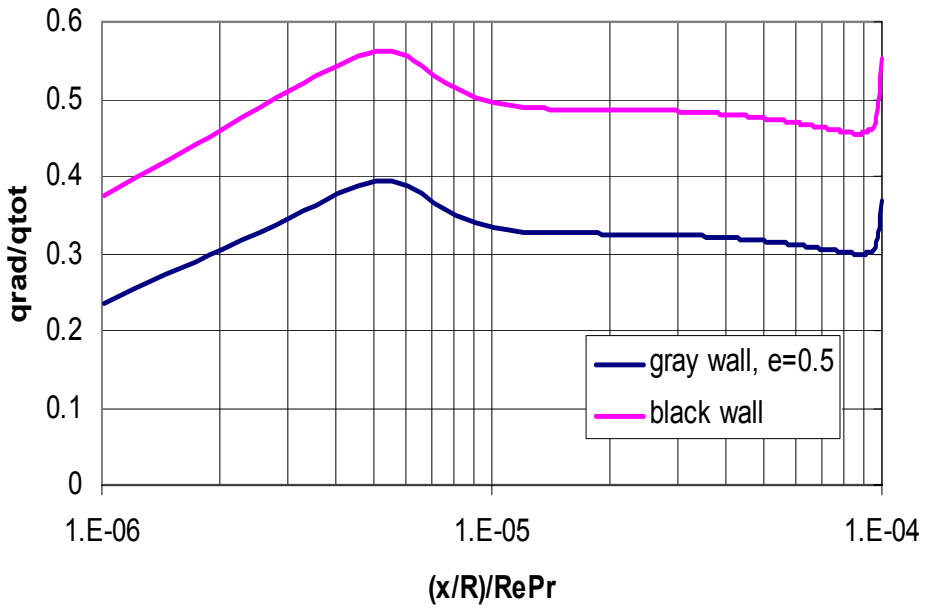

Figure 23. Relative Contribution of the Radiative Heat Flux in Different Wall Emissivities

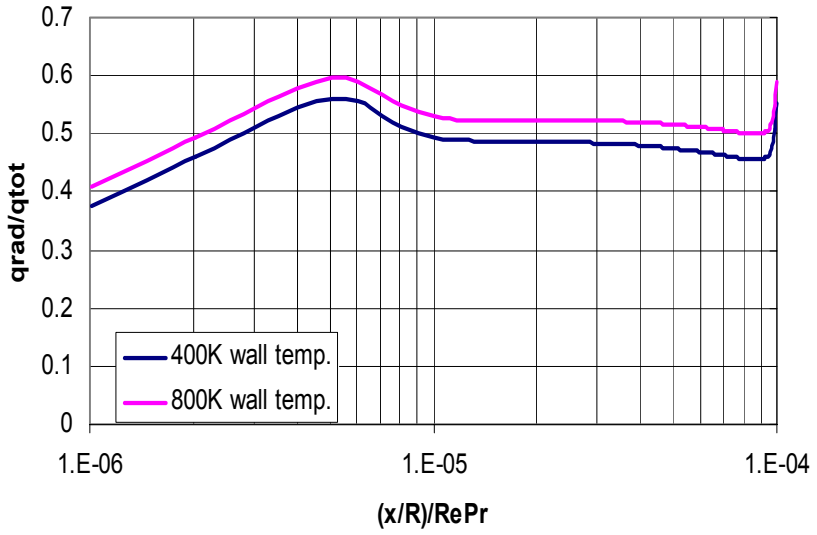

Figure 24. Relative Contribution of the Radiative Heat Flux in Different Wall Emissivities

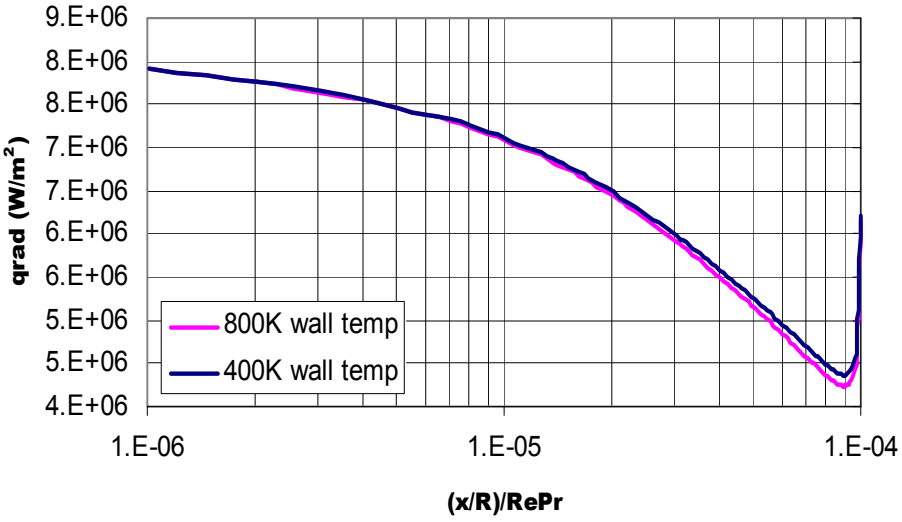

Figure 25. Relative Contribution of the Radiative Heat Flux in Different Wall Emissivities

B. NONGRAY GAS CASE

A parametric study was conducted by varying gas pressure in addition to the parameters which used in the gray gas approximation. Figure 26 shows the typical constituents in the gas mixture resulting from the complete combustion of RP1 fuel with oxygen as oxidant and an O/F ratio of 3.0. Figure 26 is for the particular gas of a 1500 K gas mixture at a pressure of 25 atmospheres.

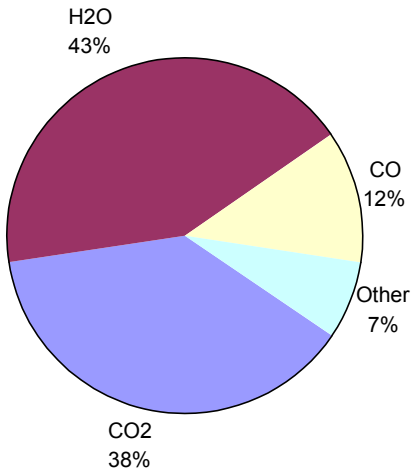

Figure 26. Typical Mole Fraction of A Gas Mixture

These mole fractions are used as input in RADCAL and to obtain spectral radiation data as shown in Figure 27 where transmissivity is plotted versus wavelength. The bandwidth of each constituent is divided into wavenumbers.

The Figures 28 and 29 discuss inlet and outlet emissivity and show the radiative heat flux to the wall for low gas to wall temperature ratio, and for high gas to wall

temperature ratio at a chamber pressure of 35 atmosphere. The blue line is for black inlet & outlet surfaces, for which the radiative heat flux is a maximum.

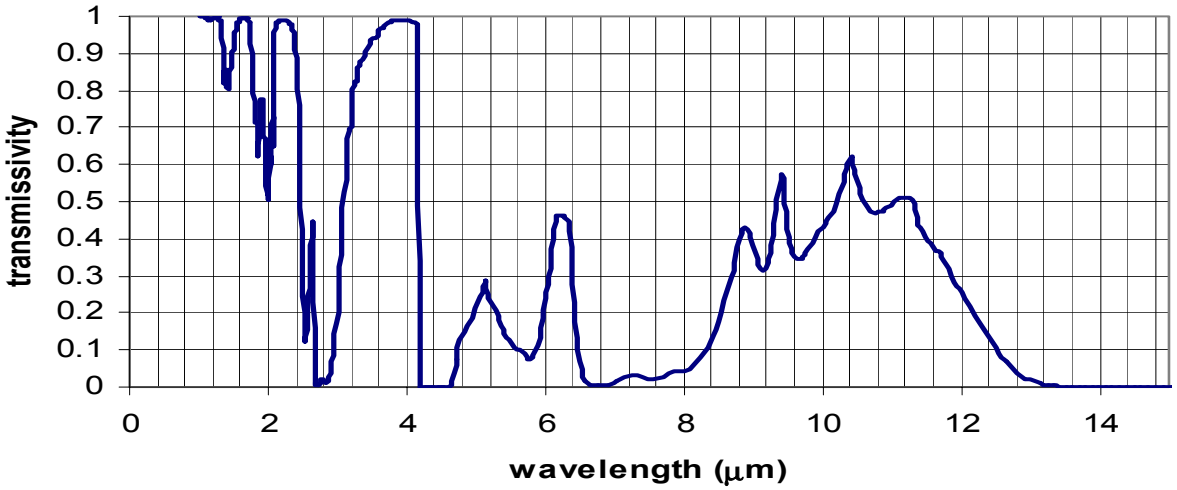

Figure 27. Typical Spectral Transmissivity

Variation of the Mixture

The purple line is for the case of zero inlet/outlet emissivity and shows only the core gas contribution. The 0.5 emissivity curve is an intermediate result between the previous cases.

Figures 30 and 31 discuss the role of wall emissivity by comparing black and gray walls and show the relative contribution of the radiative heat flux versus the non-dimensional length along the duct for low gas to wall temperature ratio and high gas to wall temperature ratio at a chamber pressure of 35 atmosphere pressures.

It is clear that, the heat flux is about 50% higher to black walls, which appears to be fairly independent of the actual gas temperature.

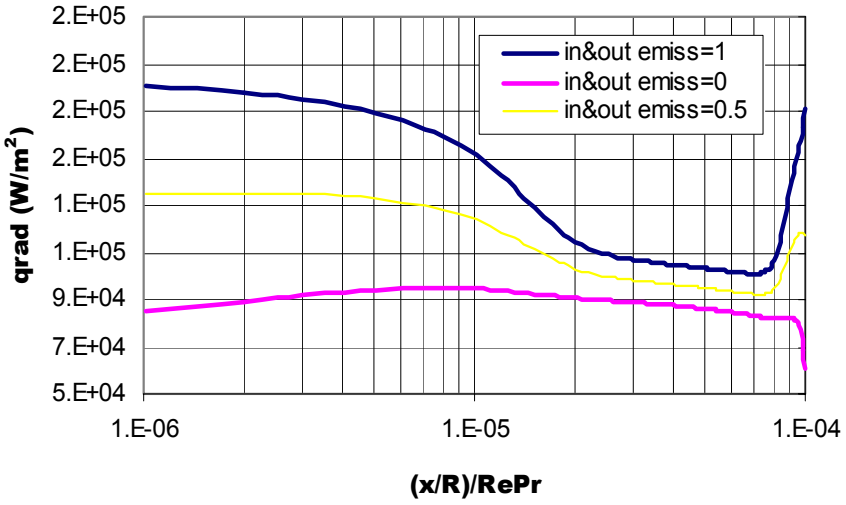

Figure 28. Heat Flux for High Gas-to-wall Temperature Ratio

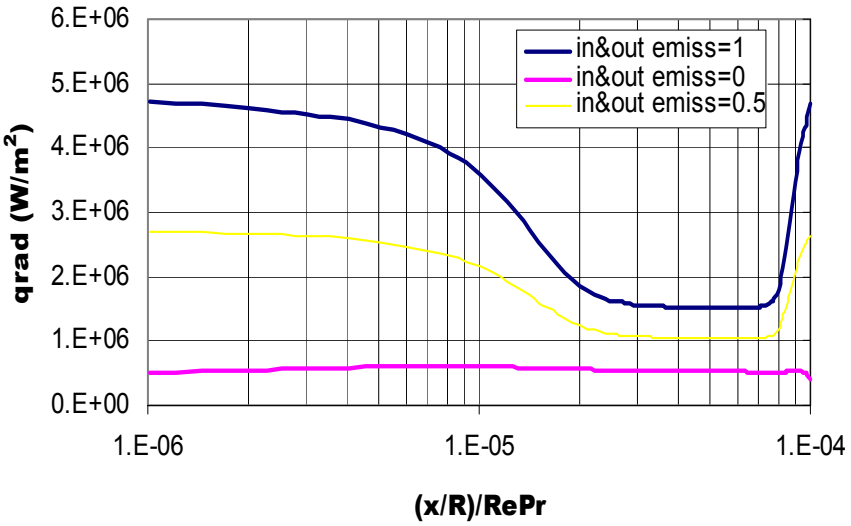

Figure 29. Heat Flux for Low Gas-to-wall Temperature Ratio

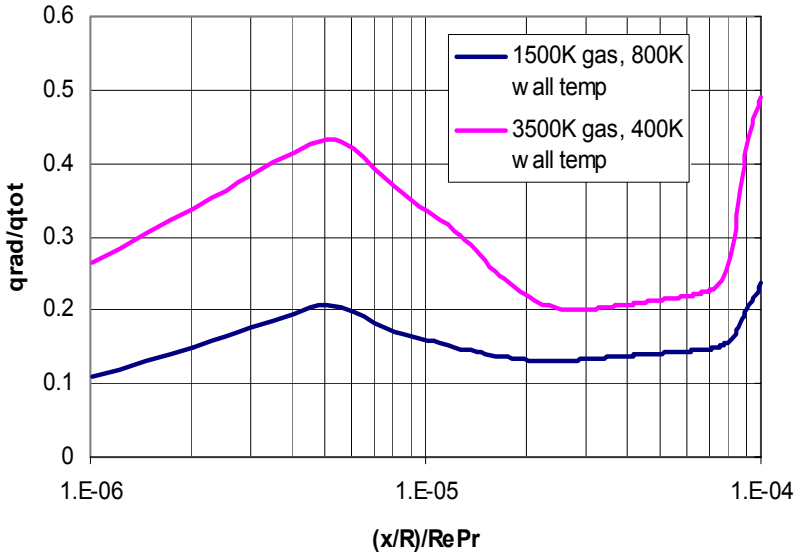

Figure 30. Heat Flux for High Gas-to-wall Temperature Ratio for Black Wall

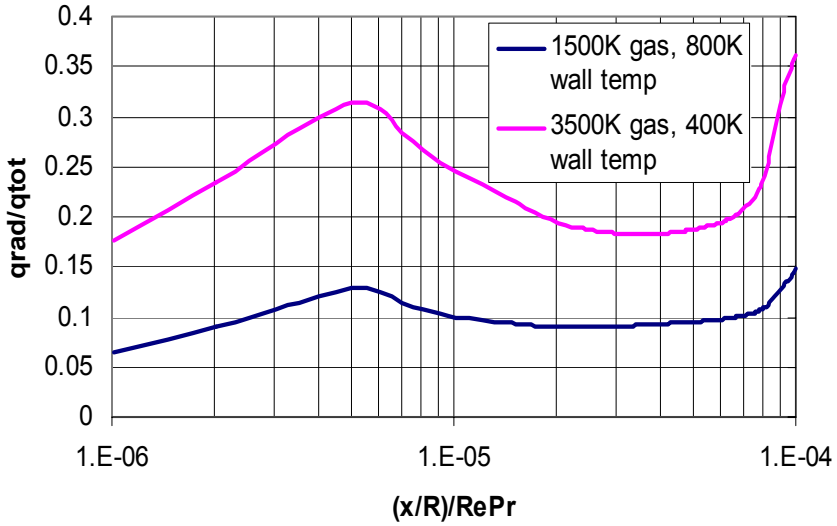

Figure 31. Heat Flux for High Gas-to-wall Temperature Ratio for Gray Wall (emissivity=0.5)

Figures 32 and 33 discuss role of gas pressure at 3500 K gas temperature and 400 K wall temperature for the case

of a black wall and show the variation of heat flux versus non-dimensional length for various chamber pressures. Both the absolute and relative values of the radiative heat flux do not change appreciably due to the fact that the absorption coefficients in the most active bands are already around their optimal value, and so much larger pressures are needed to alter the radiative heat flux significantly.

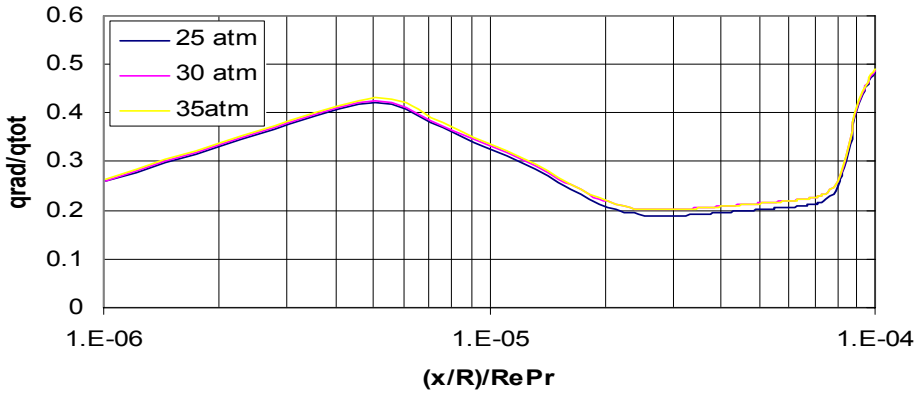

Figure 32. Relative Contribution of Heat Flux in Black Wall for Various Gas Pressures

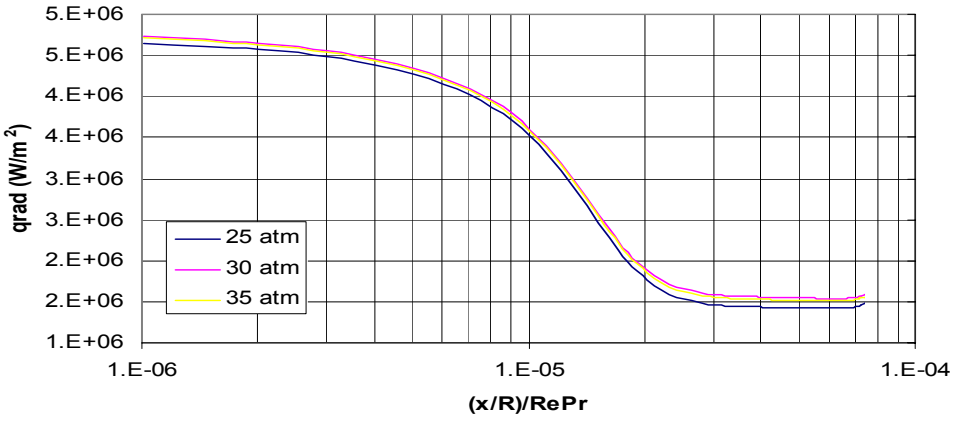

Figure 33. Radiative Heat Flux in Black wall for Various Gas Pressures

VII. CONCLUSIONS AND RECOMMENDATIONS

A numerical model has been developed for finding the radiative heat load on the walls of a combustion chamber. Such a model is useful for improving and augmenting the predictive capabilities of other numerical codes that provide only convective heat loads.

Although some of the trends in results are expected, this study provides concrete quantitative estimates of the role of gas temperature, wall temperature and emissivity, etc.

It was found that the radiative fluxes are least sensitive to the wall temperature and chamber pressure in the range considered. However, the effective emissivities of the inlet and outlet surfaces were found to be crucial in determining the magnitude of these fluxes.

Most importantly, it was found that, a proper non-gray spectral treatment of the gas mixture is critical for an accurate analysis. A gray treatment is too simplistic and yields unreliable results.

More accurate and realistic estimates can be obtained by expanding the study to include the following:

- The absorption-emission and scattering effects of particulate matter such as soot
- The role of the liquid fuel that is injected to form a film on the chamber walls

- The interaction of the combustion mechanics with the flow and heat transfer characteristics
- The effect of the resulting non-uniform distribution of gaseous species in the chamber

APPENDIX A. THE WALL CONTRIBUTION TO HEAT FLUX

If the medium is not at radiative equilibrium (i.e. conduction and/or convection is not negligible and radiative heat transfer is not dominant) the heat flux is found by using the definition of the exponential integrals in [1] as

$$q(\tau) = 2J_1E_3(\tau) - 2J_2E_3(\tau_L - \tau) + 2\sigma T_m{}^4 \int_0^{\tau} E_2(\tau - \tau')d\tau' - 2\sigma T_m{}^4 \int_{\tau}^{\tau_L} E_2(\tau' - \tau)d\tau'$$

and it becomes

$$q(\tau) = 2J_1E_3(\tau) - 2J_2E_3(\tau_L - \tau) + 2\sigma T_m{}^4[E_3(\tau) - E_3(\tau_L - \tau)]$$

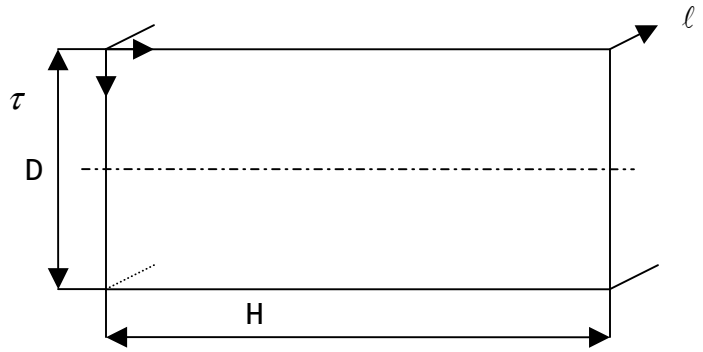

Figure 34. Optical Coordinates for the Model

As shown in Figure 34 optical coordinate at the upper wall is zero and optical coordinate at the lower wall is τ_L. Setting τ equal to zero and τ_L in the previous equation consecutively gives

$$q(0) = 2J_1E_3(0) - 2J_2E_3(\tau_L) + 2\sigma T_m{}^4[E_3(0) - E_3(\tau_L)] = \frac{\varepsilon_1}{1-\varepsilon_1}(\sigma T_1{}^4 - J_1)$$

$$q(\tau_L) = 2J_1E_3(\tau_L) - 2J_2E_3(0) + 2\sigma T_m{}^4[E_3(\tau) - E_3(0)] = \frac{\varepsilon_2}{1-\varepsilon_2}(\sigma T_2{}^4 - J_2)$$

By solving these equations simultaneously, it is found that the heat flux at the upper wall is

$$q(\tau=0)=\frac{\varepsilon_1}{1-\varepsilon_1}\left(\sigma T_1^{\,4}-\frac{\dfrac{\varepsilon_2}{1-\varepsilon_2}\sigma T_2^{\,4}-\dfrac{\dfrac{\varepsilon_1}{1-\varepsilon_1}\sigma T_1^{\,4}}{1-\dfrac{\varepsilon_1}{1-\varepsilon_1}}}{\dfrac{1}{1-\dfrac{\varepsilon_1}{1-\varepsilon_1}}-\left(1-\dfrac{\varepsilon_2}{1-\varepsilon_2}\right)}\right)$$

As seen in the equation above, the expression found for the heat flux at the upper wall considers the emissivity and temperatures of the top and bottom walls.

APPENDIX B. TYPICAL CFD-ACE OUTPUT

```
************************************************************
 **                                                        **
 **   CCCCC  FFFFF  DDDD        AAA   CCCCC  EEEEE  U   U   **
 **   C      F      D   D      A   A  C      E      U   U   **
 **   C      FFFF   D   D  ==  AAAAA  C      EEEE   U   U   **
 **   C      F      D   D      A   A  C      E      U   U   **
 **   CCCCC  F      DDDD       A   A  CCCCC  EEEEE   UUU    **
 **                                                        **
 **       Version          : 2002. 0.27                    **
 **       Build Date       : 07/28/2002 22:34:49           **
 **       Build OS         : Windows_NT                    **
 **       Build OS Release : 1.3.12(0.54/3/2)              **
 **       Build OS Version : 2002-07-06 02:16              **
 **       Build Machine    : BELL2                         **
 **                                                        **
 **      Copyright (c) 2000, CFD Research Corporation,     **
 **                  All Rights Reserved                   **
 ************************************************************

  ================================================================
   CFD-ACEU Run Platform Information :
 ================================================================
   Run Date           : 11/24/2002 15:52:48
   Run OS             : Windows
   Run OS Release     :
   Run OS Version     :
   Run Machine        : IT002099
```

```
================================================================


 ====================================
 Summary of Input Information
 ====================================
   Title              :
   Modules            : FLOW HEAT TURBULENCE RADIATION
   DTF File Name      : 3500Kgas800Kwallew05kappa3.DTF
   Model Name         : 3500Kgas800Kwallew05kappa3
   Simulation Number  :   1
   Diagnostic         : OFF
   Iterations         :   3000
   Output Frequency   :   3000
   Time Dependence    : Steady
  ====================================
  Summary of 2D Axisymmetric Grid Data
  ====================================
   Total No. of nodes :    10000
   No. of line faces  :    19800
   Total No. of faces :    19800
   No. of quad cells  :     9801
   Total No. of cells :     9801
   ====================================
  Summary of Properties
  ====================================
  Total No. of Property VCs :       1
  ====================================
   ----------------------------
   Key No.          :       41
```

```
   Zone No.          :       1

   VC Name.          : NoName

   No. of Cells      :    9801

   Material  Type    : Fluid

   Density   method : Constant      = 2.97E+00

   Viscosity method : Constant_Dyn  = 9.52E-05

   Cond.     method: Prandtl       = 6.5E-01

   Sp. Heat method: Constant      = 1.94E+03

   Absorption Coeff. Set: gas

   Emissivity Set: None
```

==========

RAD_SNORD Statistics

==========

```
Radiation Parameters

Gray model       = TRUE

CASN-DOM          = TRUE

S4 scheme        = TRUE

sn_hrange scheme  = TRUE

% Relative Error in Moments

     err_0m     = -2.980232E-06

     err_1m_mu  = -1.092752E-05

     err_1m_xi  = -1.092752E-05

     err_1m_et  = -1.000000E+02

     err_2m_mu  = -1.185405E-05

     err_2m_xi  = -1.185405E-05

     err_2m_et  = -1.185405E-05

 ====================================
```

```
 Summary of Geometry Data

 ====================================


 Smallest Volume   :   5.815956E-13

 Largest Volume   :   4.210562E-09

  Smallest Angle    :   8.999974E+01 at face =         9

  Location of face number         9 is x =   7.5061E-02 y =   1.9050E-02

 ==============================

 Start of Iterative Cycle.....

 ==============================

 Problem converged with specified criterion =   1.00E-10

 ======================================

Current Iteration # :          525

=========================================================================

 Boundary-by-Boundary Mass Flow Summary (kg/sec/rad)


=========================================================================

             Name              Key  Type        Inflow         Outflow
Sum


=========================================================================

          2  NoName                    37  Inlet        2.786166E-02
0.000000E+00   2.78617E-02

          4  NoName                    36  Outlet       0.000000E+00  -
2.786166E-02  -2.78617E-02


=========================================================================

            Total volume source
0.00000E+00

=========================================================================
```

Total Mass Flow Summary 2.786166E-02 -
2.786166E-02 -5.55112E-17

==========

==========

Force Summary at Wall Boundaries (N)

==========

Pressure Forces

==========

	Name	Key	Type	X-axis	Y-axis
1	NoName	28	Wall	0.000000E+00	4.668745E+03

==========

Shear Forces

==========

	Name	Key	Type	X-axis	Y-axis
1	NoName	28	Wall	7.307589E-02	-1.089986E-04

==========

Moment Summary at Wall Boundaries (N-m)

==========

Pressure Moments

==========

	Name	Key	Type	X-axis	Y-axis	Z-axis
1	NoName	28	Wall	0.000000E+00	0.000000E+00	1.778739E+02

==========

Viscous Moments

==========

	Name	Key	Type	X-axis	Y-axis	Z-axis
1	NoName	28	Wall	0.000000E+00	0.000000E+00	-1.392094E-03

==========

==========

Boundary-by-Boundary Heat Transfer Summary (watts/rad)

==========

Name	key	Type	COND.+CONV.	W_SRC.+CVD	RADIATION*	Sum
NoName	37	Inlet	1.8899E+05	0.0000E+00	1.2769E+02	1.8912E+05
NoName	36	Outlet	-1.7693E+05	0.0000E+00	3.6525E+02	-1.7656E+05
NoName	28	Wall	-8.2173E+03	0.0000E+00	-4.3441E+03	-1.2561E+04

==========

Total volume source

0.0000E+00

```
================================================================================

         Total Heat Imbalance      3.8479E+03   0.0000E+00  -3.8511E+03  -
3.2126E+00

================================================================================

         Total wall HEAT source
0.0000E+00

        * Radiation Summary Convention is +ve if  emmitting, -ve if absorbing.

        * Cond+Conv Summary Convention is +ve if  flux into the cell, -ve if
flux leavi ng the cell.

================================================================================

         End   of Iterative Cycle.....

================================================================================

        Final Time   Elapsed Time= 6.552923E+02 Delta-time= 6.552923E+02

        Normal Termination
```

THIS PAGE INTENTIONALLY LEFT BLANK

APPENDIX C. TYPICAL RADCAL INPUT

```
1
0.2850 1000. 7.5 15.6 .0 .0 .0 77.0 .0
0. 50. 10000.
1
1.000 1000. 7.5 15.6 .0 .0 .0 77.0 .0
0. 2000. 3000.
0
0.030 1000. 7.5 15.6 .0 .0 .0 77.0 .0
1500. 50. 10000.
1
0.010 1000. 7.5 15.6 .0 .0 .0 77.0 .0
1500. 50. 10000.
1
0.003 1000. 7.5 15.6 .0 .0 .0 77.0 .0
1500. 50. 10000.
1
0.001 1000. 7.5 15.6 .0 .0 .0 77.0 .0
1500. 50. 10000.
1
0.0003 1000. 7.5 15.6 .0 .0 .0 77.0 .0
1500. 50. 10000.
1
0.0001 1000. 7.5 15.6 .0 .0 .0 77.0 .0
1500. 50. 10000.
0
```

```
Data input file for RADCAL

line 1:  number of homogeneous elements, n
line 2:      pathlength (m), temperature (K), CO2 (kPa), H2O, CH4, CO,
O2, N2, fv
lines 3 through n+1:  same as line 2 for the rest of the elements
line n+2:  wall temperature (K), minimum wavenumber (cm-1), maximum
wavenumber
line n+3:  0, or the number of homogeneous elements in the next case
```

THIS PAGE INTENTIONALLY LEFT BLANK

APPENDIX D. TYPICAL RADCAL OUTPUT

Radial Profiles

Partial Pressures, kPa

J	dist,m	temp,K	CO2	H2O	CH4	CO	O2	N2	FV
1	.2850	1000.	7.500	15.600	.000	.000	.000	77.0	0.0
wall		400.							

Total directional radiated energy flux = .307139E+04 Watts/m-2/strad

Spectral Intensity Distribution, Watts/m-2/micron/strad

---

micron	intensity	tau	micron	intensity	tau
1.005	.0000E+00	1.0000	6.061	.2463E+03	.8353
1.010	.0000E+00	1.0000	6.154	.1477E+03	.8975
1.015	.0000E+00	1.0000	6.250	.1126E+03	.9189
1.020	.0000E+00	1.0000	6.349	.1516E+03	.8865
1.026	.0000E+00	1.0000	6.452	.3674E+03	.7137
1.031	.0000E+00	1.0000	6.557	.5144E+03	.5824
1.036	.0000E+00	1.0000	6.667	.4936E+03	.5821
1.042	.0000E+00	1.0000	6.780	.4175E+03	.6309
1.047	.0000E+00	1.0000	6.897	.3891E+03	.6404
1.053	.0000E+00	1.0000	7.018	.3447E+03	.6665
1.058	.0000E+00	1.0000	7.143	.3104E+03	.6852
1.064	.0000E+00	1.0000	7.273	.2909E+03	.6904
1.070	.0000E+00	1.0000	7.407	.2773E+03	.6897
1.075	.0000E+00	1.0000	7.547	.2674E+03	.6850
1.081	.2750E-03	1.0000	7.692	.2309E+03	.7133
1.087	.5450E-03	1.0000	7.843	.1981E+03	.7403
1.093	.5559E-02	1.0000	8.000	.1503E+03	.7915
1.099	.7908E-02	.9999	8.163	.1068E+03	.8431
1.105	.1017E-01	.9999	8.333	.7042E+02	.8902
1.111	.1929E-01	.9999	8.511	.4206E+02	.9303
1.117	.3087E-01	.9998	8.696	.2218E+02	.9608
1.124	.3884E-01	.9998	8.889	.1643E+02	.9690
1.130	.4722E-01	.9998	9.091	.2560E+02	.9484
1.136	.5675E-01	.9997	9.132	.2681E+02	.9452
1.143	.6802E-01	.9997	9.174	.2729E+02	.9434
1.149	.7338E-01	.9997	9.217	.2677E+02	.9437
1.156	.9351E-01	.9996	9.259	.2505E+02	.9466
1.163	.1019E+00	.9996	9.302	.2200E+02	.9524
1.170	.1129E+00	.9995	9.346	.1768E+02	.9612
1.176	.1128E+00	.9996	9.390	.1214E+02	.9730
1.183	.1404E+00	.9995	9.434	.1413E+02	.9681
1.190	.1451E+00	.9995	9.479	.1813E+02	.9585
1.198	.9713E-01	.9997	9.524	.2072E+02	.9519
1.205	.1105E+00	.9996	9.569	.2199E+02	.9482

1.212	.9183E-01	.9997	9.615	.2207E+02	.9472
1.220	.1101E+00	.9997	9.662	.2119E+02	.9486
1.227	.5030E-01	.9999	9.709	.1966E+02	.9515
1.235	.4276E-01	.9999	9.756	.1780E+02	.9555
1.242	.4418E-01	.9999	9.804	.1598E+02	.9594
1.250	.1951E-01	1.0000	9.852	.1440E+02	.9629
1.258	.1816E-01	1.0000	9.901	.1324E+02	.9653
1.266	.2371E-01	.9999	9.950	.1255E+02	.9666
1.274	.3800E-01	.9999	10.000	.1225E+02	.9669
1.282	.5689E-01	.9999	10.050	.1224E+02	.9664
1.290	.7012E-01	.9999	10.101	.1226E+02	.9658
1.299	.3162E+00	.9994	10.152	.1212E+02	.9657
1.307	.3513E+00	.9993	10.204	.1167E+02	.9664
1.316	.8466E+00	.9984	10.256	.1080E+02	.9684
1.325	.2019E+01	.9964	10.309	.9539E+01	.9717
1.333	.2680E+01	.9954	10.363	.7912E+01	.9761
1.342	.7485E+01	.9876	10.417	.6633E+01	.9796
1.351	.1995E+02	.9682	10.471	.8154E+01	.9746
1.361	.3008E+02	.9539	10.526	.9307E+01	.9705
1.370	.3041E+02	.9551	10.582	.1006E+02	.9676
1.379	.2758E+02	.9608	10.638	.1035E+02	.9660
1.389	.3325E+02	.9545	10.695	.1024E+02	.9658
1.399	.3583E+02	.9527	10.753	.9810E+01	.9667
1.408	.3438E+02	.9563	10.811	.9186E+01	.9683
1.418	.3388E+02	.9585	10.870	.8521E+01	.9701
1.429	.3091E+02	.9635	10.929	.7865E+01	.9719
1.439	.2601E+02	.9703	10.989	.7284E+01	.9735
1.449	.2227E+02	.9755	11.050	.6814E+01	.9748
1.460	.1790E+02	.9810	11.111	.6460E+01	.9756
1.471	.1061E+02	.9891	11.173	.6270E+01	.9759
1.481	.9673E+01	.9904	11.236	.6159E+01	.9759
1.493	.8050E+01	.9923	11.299	.6104E+01	.9757
1.504	.6925E+01	.9936	11.364	.6029E+01	.9756
1.515	.5957E+01	.9947	11.429	.6057E+01	.9750
1.527	.4139E+01	.9964	11.494	.6112E+01	.9743
1.538	.3552E+01	.9970	11.561	.6162E+01	.9736
1.550	.2128E+01	.9983	11.628	.6207E+01	.9729
1.563	.1522E+01	.9988	11.696	.6248E+01	.9722
1.575	.1290E+01	.9990	11.765	.6283E+01	.9715
1.587	.1014E+01	.9993	11.834	.6376E+01	.9705
1.600	.6685E+00	.9995	11.905	.6463E+01	.9695
1.613	.4852E+00	.9997	11.976	.6542E+01	.9685
1.626	.4411E+00	.9997	12.048	.7069E+01	.9653
1.639	.4084E+00	.9997	12.121	.7273E+01	.9636
1.653	.3866E+00	.9998	12.195	.9147E+01	.9533
1.667	.3688E+00	.9998	12.270	.8254E+01	.9570
1.681	.4618E+00	.9997	12.346	.8842E+01	.9530
1.695	.5073E+00	.9997	12.422	.9667E+01	.9475
1.709	.6027E+00	.9997	12.500	.1025E+02	.9432
1.724	.1392E+01	.9993	12.579	.1104E+02	.9376
1.739	.3258E+01	.9983	12.658	.1197E+02	.9309
1.754	.9787E+01	.9950	12.739	.1348E+02	.9205
1.770	.2302E+02	.9886	12.821	.1497E+02	.9098

1.786	.4804E+02	.9769	12.903	.1582E+02	.9026
1.802	.8527E+02	.9601	12.987	.1767E+02	.8888
1.818	.1165E+03	.9469	13.072	.1978E+02	.8728
1.835	.1231E+03	.9453	13.158	.2243E+02	.8526
1.852	.1330E+03	.9424	13.245	.2550E+02	.8286
1.869	.1840E+03	.9224	13.333	.2466E+02	.8305
1.887	.1082E+03	.9555	13.423	.3142E+02	.7792
1.905	.8995E+02	.9639	13.514	.3864E+02	.7222
1.923	.1072E+03	.9580	13.605	.3805E+02	.7201
1.942	.1342E+03	.9487	13.699	.3886E+02	.7074
1.961	.1511E+03	.9435	13.793	.4769E+02	.6325
1.980	.1217E+03	.9555	13.889	.7088E+02	.4409
2.000	.1395E+03	.9501	13.986	.6696E+02	.4591
2.010	.9192E+02	.9675	14.085	.6327E+02	.4766
2.020	.8857E+02	.9690	14.184	.6714E+02	.4310
2.030	.4371E+02	.9849	14.286	.6781E+02	.4113
2.041	.4465E+02	.9847	14.388	.7217E+02	.3579
2.051	.4845E+02	.9836	14.493	.7992E+02	.2711
2.062	.3829E+02	.9872	14.599	.8159E+02	.2371
2.073	.4135E+02	.9863	14.706	.7775E+02	.2545
2.083	.1168E+02	.9962	14.815	.8612E+02	.1531
2.094	.4225E+01	.9986	14.925	.9416E+02	.0500
2.105	.1757E+01	.9994	15.038	.9091E+02	.0589
2.116	.1581E+01	.9995	15.152	.6921E+02	.2646
2.128	.1470E+01	.9995	15.267	.6953E+02	.2416
2.139	.1308E+01	.9996	15.385	.6904E+02	.2267
2.151	.1150E+01	.9996	15.504	.5944E+02	.3162
2.162	.1113E+01	.9997	15.625	.5130E+02	.3937
2.174	.1056E+01	.9997	15.748	.4844E+02	.4116
2.186	.1081E+01	.9997	15.873	.4464E+02	.4427
2.198	.1131E+01	.9997	16.000	.3964E+02	.4913
2.210	.1246E+01	.9996	16.129	.3698E+02	.5119
2.222	.1342E+01	.9996	16.260	.4188E+02	.4313
2.235	.1390E+01	.9996	16.393	.3814E+02	.4672
2.247	.2010E+01	.9994	16.529	.3307E+02	.5245
2.260	.2084E+01	.9994	16.667	.3046E+02	.5491
2.273	.2685E+01	.9992	16.807	.3175E+02	.5159
2.286	.3155E+01	.9991	16.949	.2961E+02	.5350
2.299	.4134E+01	.9988	17.094	.2789E+02	.5486
2.312	.4731E+01	.9987	17.241	.2691E+02	.5512
2.326	.6020E+01	.9983	17.391	.2615E+02	.5503
2.339	.6801E+01	.9981	17.544	.2582E+02	.5421
2.353	.8293E+01	.9977	17.699	.2576E+02	.5287
2.367	.9228E+01	.9975	17.857	.2516E+02	.5249
2.381	.1570E+02	.9958	18.018	.2490E+02	.5147
2.395	.1983E+02	.9947	18.182	.2457E+02	.5054
2.410	.3383E+02	.9910	18.349	.2429E+02	.4950
2.424	.5294E+02	.9860	18.519	.2388E+02	.4869
2.439	.9285E+02	.9755	18.692	.2350E+02	.4780
2.454	.1579E+03	.9586	18.868	.2298E+02	.4722
2.469	.2717E+03	.9291	19.048	.2256E+02	.4641
2.484	.4305E+03	.8883	19.231	.2215E+02	.4556
2.500	.6355E+03	.8359	19.417	.2176E+02	.4462

2.516	.8206E+03	.7891	19.608	.2134E+02	.4374
2.532	.9776E+03	.7500	19.802	.2090E+02	.4293
2.548	.1067E+04	.7282	20.000	.2043E+02	.4217
2.564	.9858E+03	.7500	20.202	.1998E+02	.4136
2.581	.1036E+04	.7384	20.408	.1952E+02	.4060
2.597	.7898E+03	.8012	20.619	.1903E+02	.3989
2.614	.7146E+03	.8208	20.833	.1853E+02	.3923
2.632	.5482E+03	.8630	21.053	.1803E+02	.3861
2.649	.4264E+03	.8938	21.277	.1755E+02	.3790
2.667	.1657E+04	.5883	21.505	.1706E+02	.3724
2.685	.1849E+04	.5419	21.739	.1657E+02	.3662
2.703	.1975E+04	.5117	21.978	.1607E+02	.3603
2.721	.1645E+04	.5943	22.222	.1557E+02	.3549
2.740	.1340E+04	.6702	22.472	.1506E+02	.3499
2.759	.1206E+04	.7038	22.727	.1456E+02	.3452
2.778	.1376E+04	.6625	22.989	.1406E+02	.3408
2.797	.1440E+04	.6473	23.256	.1356E+02	.3366
2.817	.1471E+04	.6400	23.529	.1307E+02	.3326
2.837	.1373E+04	.6642	23.810	.1258E+02	.3291
2.857	.1190E+04	.7092	24.096	.1210E+02	.3258
2.878	.9948E+03	.7570	24.390	.1163E+02	.3226
2.899	.8855E+03	.7837	24.691	.1116E+02	.3196
2.920	.7522E+03	.8163	25.000	.1071E+02	.3168
2.941	.6446E+03	.8425	25.316	.1025E+02	.3150
2.963	.5486E+03	.8659	25.641	.9802E+01	.3134
2.985	.4688E+03	.8853	25.974	.9368E+01	.3117
3.008	.3842E+03	.9059	26.316	.8945E+01	.3102
3.030	.3267E+03	.9198	26.667	.8535E+01	.3088
3.053	.2719E+03	.9332	27.027	.8122E+01	.3086
3.077	.2190E+03	.9461	27.397	.7724E+01	.3085
3.101	.1660E+03	.9590	27.778	.7339E+01	.3084
3.125	.1280E+03	.9683	28.169	.6967E+01	.3083
3.150	.1127E+03	.9720	28.571	.6610E+01	.3082
3.175	.9436E+02	.9765	28.986	.6254E+01	.3094
3.200	.7517E+02	.9812	29.412	.5913E+01	.3105
3.226	.6378E+02	.9840	29.851	.5585E+01	.3116
3.252	.5180E+02	.9870	30.303	.5271E+01	.3127
3.279	.4519E+02	.9886	30.769	.4971E+01	.3137
3.306	.3939E+02	.9900	31.250	.4673E+01	.3162
3.333	.3259E+02	.9917	31.746	.4389E+01	.3186
3.361	.2895E+02	.9926	32.258	.4118E+01	.3210
3.390	.2597E+02	.9933	32.787	.3860E+01	.3234
3.419	.2072E+02	.9946	33.333	.3615E+01	.3258
3.448	.1764E+02	.9954	33.898	.3374E+01	.3295
3.478	.1464E+02	.9961	34.483	.3145E+01	.3333
3.509	.1238E+02	.9967	35.088	.2928E+01	.3371
3.540	.1063E+02	.9972	35.714	.2723E+01	.3408
3.571	.8686E+01	.9977	36.364	.2529E+01	.3445
3.604	.6410E+01	.9983	37.037	.2338E+01	.3505
3.636	.4385E+01	.9988	37.736	.2158E+01	.3565
3.670	.3877E+01	.9989	38.462	.1988E+01	.3626
3.704	.3277E+01	.9991	39.216	.1829E+01	.3687
3.738	.2320E+01	.9993	40.000	.1679E+01	.3749

3.774	.2023E+01	.9994	40.816	.1534E+01	.3832
3.810	.1604E+01	.9995	41.667	.1398E+01	.3918
3.846	.1533E+01	.9996	42.553	.1272E+01	.4005
3.883	.1524E+01	.9996	43.478	.1154E+01	.4095
3.922	.1518E+01	.9995	44.444	.1044E+01	.4187
3.960	.1460E+01	.9996	45.455	.9412E+00	.4290
4.000	.1480E+01	.9995	46.512	.8458E+00	.4395
4.040	.1690E+01	.9995	47.619	.7576E+00	.4505
4.082	.1985E+01	.9994	48.780	.6763E+00	.4619
4.124	.2304E+01	.9993	50.000	.6015E+00	.4737
4.167	.2646E+01	.9991	51.282	.5334E+00	.4855
4.211	.2953E+04	.0324	52.632	.4711E+00	.4978
4.255	.2995E+04	.0031	54.054	.4141E+00	.5106
4.301	.2954E+04	.0008	55.556	.3623E+00	.5241
4.348	.2905E+04	.0006	57.143	.3152E+00	.5383
4.396	.2846E+04	.0039	58.824	.2731E+00	.5525
4.444	.2625E+04	.0648	60.606	.2351E+00	.5675
4.494	.1643E+04	.4038	62.500	.2009E+00	.5835
4.545	.5766E+03	.7868	64.516	.1703E+00	.6006
4.598	.1604E+03	.9395	66.667	.1430E+00	.6190
4.651	.7032E+02	.9729	68.966	.1200E+00	.6354
4.706	.6562E+02	.9742	71.429	.9956E-01	.6531
4.762	.8193E+02	.9671	74.074	.8162E-01	.6723
4.819	.9943E+02	.9592	76.923	.6593E-01	.6933
4.878	.1257E+03	.9472	80.000	.5227E-01	.7166
4.938	.1503E+03	.9354	83.333	.4202E-01	.7328
5.000	.1674E+03	.9263	86.957	.3324E-01	.7503
5.063	.1852E+03	.9164	90.909	.2578E-01	.7695
5.128	.1905E+03	.9118	95.238	.1949E-01	.7909
5.195	.2603E+03	.8764	100.000	.1424E-01	.8150
5.263	.2817E+03	.8625	105.263	.1073E-01	.8295
5.333	.3009E+03	.8491	111.111	.7875E-02	.8452
5.405	.3575E+03	.8155	117.647	.5586E-02	.8625
5.479	.3563E+03	.8106	125.000	.3781E-02	.8818
5.556	.4000E+03	.7808	133.333	.2387E-02	.9038
5.634	.4012E+03	.7733	142.857	.1644E-02	.9130
5.714	.4043E+03	.7642	153.846	.1088E-02	.9228
5.797	.4231E+03	.7450	166.667	.6855E-03	.9333
5.882	.3710E+03	.7687	181.818	.4039E-03	.9445
5.970	.2889E+03	.8135	200.000	.2162E-03	.9567

The effective absorption coef. is .654587E+00/m
The Planck-mean absorption coef. is .290665E+01/m
The wall-incident mean is .290665E+01/m

Radial Profiles

Partial Pressures, kPa

```
  J  dist,m   temp,K   CO2     H2O     CH4     CO      O2      N2
FV
  1   1.0000  1000.   7.500  15.600    .000    .000    .000  77.000
.0000E+00
wall             0.
```

Total directional radiated energy flux = .125184E+04 Watts/m-2/strad

Spectral Intensity Distribution, Watts/m-2/micron/strad

micron	intensity	tau	micron	intensity	tau
3.339	.1085E+03	.9723	4.008	.5337E+01	.9984
3.367	.9697E+02	.9751	4.049	.6130E+01	.9981
3.396	.8553E+02	.9779	4.090	.7178E+01	.9977
3.425	.6933E+02	.9820	4.132	.8308E+01	.9974
3.454	.5894E+02	.9846	4.175	.2151E+04	.3038
3.484	.4918E+02	.9870	4.219	.3041E+04	.0006
3.515	.4178E+02	.9889	4.264	.2995E+04	.0000
3.546	.3564E+02	.9905	4.310	.2947E+04	.0000
3.578	.2868E+02	.9923	4.357	.2897E+04	.0000
3.610	.2096E+02	.9943	4.405	.2847E+04	.0000
3.643	.1498E+02	.9959	4.454	.2793E+04	.0012
3.676	.1314E+02	.9964	4.505	.2490E+04	.0932
3.711	.1080E+02	.9970	4.556	.1262E+04	.5315
3.745	.7920E+01	.9978	4.608	.4181E+03	.8417
3.781	.6793E+01	.9981	4.662	.2144E+03	.9172
3.817	.5574E+01	.9984	4.717	.2115E+03	.9166
3.854	.5368E+01	.9984	4.773	.2523E+03	.8983
3.891	.5338E+01	.9984	4.831	.2964E+03	.8778
3.929	.5280E+01	.9984	4.890	.3505E+03	.8522
3.968	.5131E+01	.9985	4.950	.3933E+03	.8302

The effective absorption coef. is .718888E-01/m
The Planck-mean absorption coef. is .199213E+01/m
The wall-incident mean is .199213E+01/m

APPENDIX E. TYPICAL TEP OUTPUT

```
INPUT FILE:D:\PC_TEP\tep.dat
OUPUT FILE:D:\PC_TEP\tep.out
THERMODYNAMIC DATA FILE:D:\PC_TEP\species\chno.dat
 TITLE RPI/GO2
 DATA
  $DATA
  ODE=1,
  NZONES=1,
  ASUB(1)=2,
  NASUB=1,
  ASUP(1)=6,
  NASUP=1,
  $END
 REACTANTS
 C 1.     H 1.9423                              100.    -5430.L  298.15F  .773
 O 2.                                           100.       0.0G  298.15O

 NAMELISTS
  $ODE
  RKT = .TRUE.
  PSIA=F,
  T(1)=1500,
  P(1)=25,
  OFSKED(1)=3,
  OF= T,
  $END

0TITLE RPI/GO2
0DATA
      $DATA
      ODE=1,
      NZONES=1,
      ASUB(1)=2,
      NASUB=1,
      ASUP(1)=6,
      NASUP=1,
      $END
1



*************************************************************************************************
*****************

                    CALCULATE ODE AREA RATIO AND PRESSURE SCHEDULES FOR ZONE  1

*************************************************************************************************
*****************
 REACTANTS
 C   1.0000  H   1.9423      0.0000      0.0000      0.0000  100.000000      -5430.00  L   298.150  F
0.77300
 O   2.0000      0.0000      0.0000      0.0000      0.0000  100.000000          0.00  G   298.150  O
0.00000
 NAMELISTS
      $ODE
      RKT = .TRUE.
      PSIA=F,
      T(1)=1500,
      P(1)=25,
      OFSKED(1)=3,
      OF= T,
      $END
0SPECIES BEING CONSIDERED IN THIS SYSTEM
     J 3/78  C                J12/67  CH               L 5/84  CH4              J 9/65  CO
J 9/65  CO2
     J12/69  C2               J 3/61  C2H2             J12/69  C3               J12/69  C4
L 6/88  JET-A(G)
     DR   9  C12H26           J 3/77   H               J12/70  HCO              J 9/78  HO2
J 3/77  H2
```

```
     J 3/79  H2O             L 6/80  H2O2            J 3/77  O               J 6/77  OH
J 3/77  O2
     J 3/78  C(GR)           J 3/79  H2O(L)            Est.  JP10(L)         L 6/88  JET-A(L)
P1   9  C12H26(L)
0OF =   3.000000
                          EFFECTIVE FUEL          EFFECTIVE OXIDANT           MIXTURE
 ENTHALPY                     HPP(2)                  HPP(1)                   HSUB0
 (KG-MOL)(DEG K)/KG      -0.19573987E+03          0.00000000E+00          -0.48934967E+02
0KG-ATOMS/KG                 B0P(I,2)                B0P(I,1)                 B0(I)
        C                 0.71587443E-01          0.00000000E+00           0.17896861E-01
        H                 0.13904428E+00          0.00000000E+00           0.34761071E-01
        O                 0.00000000E+00          0.62502339E-01           0.46876755E-01

 ENTHALPY IN BTU/LBM :
     FROM REACTANTS :       -174.9239
     FROM DELH( )   :          0.0000
     FROM DELH1( )             0.0000
     TOTAL          :       -174.9239
1                                                  ZONE =  1
                        THEORETICAL ROCKET PERFORMANCE ASSUMING EQUILIBRIUM COMPOSITION DURING
EXPANSION

                                              FROM AN ASSIGNED PRESSURE AND TEMPERATURE
0PC =   367.4 PSIA
                                                                                        WT FRACTION  ENTHALPY
STATE   TEMP    DENSITY
          CHEMICAL FORMULA                                                              (SEE NOTE)    CAL/MOL
DEG K    G/CC
 FUEL    C  1.00000   H  1.94230                                                          1.00000    -5430.000
L    298.15   0.7730
 OXIDANT O  2.00000                                                                     1.00000        0.000
G    298.15   0.0000
0O/F=3.0000E+00  PERCENT FUEL=2.5000E+01  EQUIVALENCE RATIO=1.1343E+00  STOIC MIXTURE RATIO=3.4030E+00
DENSITY=0.0000E+00
0                CHAMBER   THROAT     EXIT     EXIT
 PC/P             1.0000   1.7704   1.0598   39.796
 P, ATM            25.00    14.12    23.59   0.6282
 T, DEG K           1500     1365     1486      822
 H, CAL/G        -1845.1  -1902.4  -1851.2  -2135.1
 S, CAL/(G)(K)    2.0645   2.0645   2.0645   2.0645
 G, CAL/GRAM     -4941.9  -4721.1  -4918.6  -3832.8
 U, CAL/GRAM     -1950.2  -1998.1  -1955.3  -2192.6
 DEN (G/LITER)  5.76E+00 3.57E+00 5.48E+00 2.65E-01

 M, MOL WT        28.347   28.347   28.347   28.427
 (DLV/DLP)T     -1.00000 -1.00000 -1.00000 -1.00502
 (DLV/DLT)P       1.0000   1.0000   1.0000   1.0833
 CP, CAL/(G)(K)   0.4269   0.4239   0.4265   0.5189
 CP GAS(SF)       0.4137   0.4057   0.4129   0.3650
 GAMMA GAS(SF)    1.2039   1.2087   1.2043   1.2367
 GAMMA (S)        1.1963   1.1980   1.1965   1.1806
 SON VEL,M/SEC     725.5    692.6    722.1    532.9
 MU, POISE      5.24E-04 4.89E-04 5.20E-04 3.32E-04
 K,ERG/S-CM-K   1.41E+04 1.30E+04 1.40E+04 8.75E+03
 PRANDTL NO      0.64509  0.63850  0.64448  0.57932
 MACH NUMBER      0.0000   1.0000   0.3124   2.9246

 AE/AT                     1.0000   2.0000   6.0001
 CSTAR, FT/SEC               3358     3358     3358
 CF  VAC                    1.242            1.673
 CF                         0.677            1.522
 IVAC,LBF-S/LBM            129.58           174.65
 I, LBF-SEC/LBM             70.63           158.91
 MOL WT(MIX)      28.347   28.347   28.347   28.427

 MOLE FRACTIONS

 CH4            0.000000 0.000000 0.000000 0.001415
 CO             0.123704 0.115658 0.122957 0.044893
 CO2            0.383614 0.391660 0.384361 0.462446
  H             0.000001 0.000000 0.000001 0.000000
 H2             0.054809 0.062854 0.055556 0.128465
 H2O            0.437872 0.429827 0.437125 0.362781

 MASS FRACTIONS
```

```
 CH4            0.000000 0.000000 0.000000 0.000799
 CO             0.122237 0.114286 0.121499 0.044235
 CO2            0.595582 0.608074 0.596742 0.715947
  H             0.000000 0.000000 0.000000 0.000000
 H2             0.003898 0.004470 0.003951 0.009110
 H2O            0.278283 0.273170 0.277808 0.229909
0ADDITIONAL PRODUCTS WHICH WERE CONSIDERED BUT WHOSE MOLE FRACTIONS WERE LESS THAN .0000005 FOR ALL
ASSIGNED CONDITIONS
 C              CH             C2             C2H2           C3             C4             JET-A(G)       C12H26
HCO            HO2
 H2O2           O              OH             O2             C(GR)          H2O(L)         JP10(L)        JET-A(L)
C12H26(L)

 NOTE
       WEIGHT FRACTION OF FUEL IN TOTAL FUELS AND OF OXIDANT IN TOTAL OXIDANTS
       (SF) STANDS FOR (SHIFTING FROZEN)
1
0                        FROZEN TRANSPORT PROPERTIES CALCULATED FROM EQUILIBRIUM CONCENTRATIONS

     STATION                    MU                  K                   PR
                          (LBF-SEC/FT**2)    (LBF/SEC-DEG R)
     CHAMBER             1.09539496E-06      1.75734852E-02      6.45086110E-01
     THROAT              1.02199533E-06      1.62469596E-02      6.38496220E-01
     EXIT                6.93548600E-07      1.09325694E-02      5.79323411E-01
0   VISCOSITY EXPONENT (OMEGA) FOR THE FORM MU=MUREF*(T/TREF)**OMEGA IS     0.76373
    MUREF FOR INPUT TO BLM=   3.53317955E-05 LBM/(FT-SEC)
0          SPECIES CONSIDERED IN TRANSPORT PROPERTIES CALCULATIONS
          C                   CH                  CH4                 CO
          CO2                 C2                  C2H2                H2
          H2O                 H2O2                O                   OH
          O2
1                                                    ZONE =  1
                         THEORETICAL ROCKET PERFORMANCE ASSUMING FROZEN COMPOSITION DURING EXPANSION

                                              FROM AN ASSIGNED PRESSURE AND TEMPERATURE
0PC =   367.4 PSIA
                                                                                          WT FRACTION  ENTHALPY
STATE   TEMP    DENSITY
          CHEMICAL FORMULA                                                                (SEE NOTE)    CAL/MOL
DEG K    G/CC
 FUEL    C  1.00000   H  1.94230                                                           1.00000    -5430.000
L    298.15   0.7730
 OXIDANT O  2.00000                                                                       1.00000        0.000
G    298.15   0.0000
0O/F=3.0000E+00  PERCENT FUEL=2.5000E+01  EQUIVALENCE RATIO=1.1343E+00  STOIC MIXTURE RATIO=3.4030E+00
DENSITY=0.0000E+00
0               CHAMBER   THROAT     EXIT     EXIT
 PC/P            1.0000   1.7776   1.0602   43.153
 P, ATM           25.00    14.06    23.58   0.5793
 T, DEG K          1500     1359     1485      752
 H, CAL/G        -1845.1  -1902.7  -1851.2  -2133.5
 S, CAL/(G)(K)    2.0645   2.0645   2.0645   2.0645
 G, CAL/GRAM     -4941.9  -4709.1  -4917.5  -3686.0
 U, CAL/GRAM     -1950.2  -1997.9  -1955.3  -2186.2
 DEN (G/LITER)  5.76E+00 3.57E+00 5.48E+00 2.66E-01

 M, MOL WT        28.347   28.347   28.347   28.347
 CP, CAL/(G)(K)   0.4137   0.4047   0.4128   0.3507
 GAMMA (S)        1.2039   1.2093   1.2044   1.2496
 SON VEL,M/SEC     727.8    694.4    724.3    525.0
 MACH NUMBER      0.0000   1.0000   0.3124   2.9602

 AE/AT                     1.0000   2.0000   6.0002
 CSTAR, FT/SEC               3349     3349     3349
 CF  VAC                    1.243             1.661
 CF                         0.680             1.523
 IVAC,LBF-S/LBM            129.36            172.94
 I, LBF-SEC/LBM             70.81            158.47

 MOLE FRACTIONS

 CO           0.123704       CO2          0.383614        H           0.000001       H2
0.054809
```

```
 H2O          0.437872

 MASS FRACTIONS


 CO           0.122237       CO2          0.595582       H2           0.003898       H2O
0.278283
0ADDITIONAL PRODUCTS WHICH WERE CONSIDERED BUT WHOSE MOLE FRACTIONS WERE LESS THAN .0000005 FOR ALL
ASSIGNED CONDITIONS
 C            CH           C2           C2H2         C3           C4           JET-A(G)     C12H26
HCO          HO2
 H2O2         O            OH           O2           C(GR)        H2O(L)       JP10(L)      JET-A(L)
C12H26(L)

 NOTE
        WEIGHT FRACTION OF FUEL IN TOTAL FUELS AND OF OXIDANT IN TOTAL OXIDANTS
1


********************************************************************************************************
******************

                    CALCULATE ODE AREA RATIO AND PRESSURE SCHEDULES FOR ZONE  1

********************************************************************************************************
******************

 *** EOF ENCOUNTERED IN READING ODE REACTANTS DATA ***

          *********CPU(SEC) =             0.0 **********
```

LIST OF REFERENCES

1. Modest, Michael F., ***Radiative Heat Transfer,*** McGraw Hill Inc., 1993.

2. Desoto, Simon, ***Coupled Radiation, Conduction and Convection in Entrance Region Flow***, International Journal of Heat and Mass Transfer, Vol 11, pp. 39-53, 1968

3. Grosshandler, William L., ***A Narrow-Band Model for Radiation Calculations in a Combustion Environment***, National Institute of Standards and Technology Technical Note 1402, 1993

4. Emery, A. F., Pearce B. E., ***Heat Transfer by Thermal Radiation and Laminar Forced Convection to an Absorbing Fluid in the Entry Region of a Pipe,*** Journal of Heat Transfer, May 1970

5. Tabanfar, S., Modest, M.F., ***Combined Radiation and Convection in Absorbing, Emitting, Non-gray Gray-Particulate Tube Flow***, Journal of Heat Transfer, May 1987

6. Azad, F.H., ***Combined Radiation and Convection in Absorbing, Emitting and Isotropically Scattering Gas-Particulate Tube Flow***, Journal of Heat Transfer, vol.24, 1981

7. Smith, T.F., Shen, Z.F., Alturki, A.M., ***Radiative and Convective Transfer in a Cylindirical Enclosure for a Real Gas***, Journal of Heat Transfer, vol.107, May 1985

8. Yener, Y., Ozisik, M.N., ***Simultaneous Radiation and Forced Convection in Thermally Developing Turbulent Flow***

Through a Parallel-Plate Channel, Journal of Heat Transfer, vol.108, November 1986

9. CFDRD Research Corporation, ***CFD-ACE User Manuel Version 2002***, 2002

INITIAL DISTRIBUTION LIST

1. Defense Technical Information Center
   Ft. Belvoir, VA

2. Dudley Knox Library
   Naval Postgraduate School
   Monterey, CA

3. Chairman, Code ME
   Department of Mechanical Engineering
   Naval Postgraduate School
   Monterey, CA

4. Engineering and Technology Curricular Office, Code 34
   Naval Postgraduate School
   Monterey, CA

5. Professor Ashok Gopinath, Code ME/Gk
   Naval Postgraduate School
   Monterey, CA

6. Dr. Christopher M. Brophy, Code AA/Br
   Department of Aeronautics and Astronautics
   Naval Postgraduate School
   Monterey, CA

7. LTJG Mehmet Koray Savur
   Naval Postgraduate School
   Monterey, CA